

1 Measurement report: Nocturnal subsidence behind the cold 2 front enhances surface particulate matter in the plain regions: 3 observation from the mobile multi-lidar system

4 Yiming Wang^{1, 2}, Haolin Wang^{1, 2}, Yujie Qin^{1, 2}, Xinqi Xu^{1, 2}, Guowen He^{1, 2}, Nanxi Liu^{1, 2}, Shengjie
5 Miao^{1, 2}, Xiao Lu^{1, 2}, Haichao Wang^{1, 2, *}, Shaojia Fan^{1, 2, *}

6 ¹School of Atmospheric Sciences, Sun Yat-sen University, and Southern Marine Science and
7 Engineering Guangdong Laboratory (Zhuhai), Zhuhai, 519082, China

8 ²Guangdong Provincial Observation and Research Station for Climate Environment and Air Quality
9 Change in the Pearl River Estuary, Key Laboratory of Tropical Atmosphere-Ocean System (Sun Yat-sen
10 University), Ministry of Education, Zhuhai, 519082, China

11 *Correspondence to:*

12 *Haichao Wang (wanghch27@mail.sysu.edu.cn); Shaojia Fan (eesfsj@mail.sysu.edu.cn)*

13 **Abstract.** A multi-lidar system, mounted in [a](#) vehicle to monitor the profiles of temperature, wind, and
14 particle optical properties, was utilized to investigate the winter fine particulate matter (PM_{2.5}) pollution
15 ~~for~~ [from](#) a vertical perspective, in four cities in China in winter 2018. We observed the enhancement of
16 surface nocturnal PM_{2.5} in two typical plain cities (Changzhou and Wangdu), which was attributed to the
17 subsidence of PM_{2.5} transported from upstream polluted areas, with the wind turning north and
18 downdrafts dominating. Combining with the observed surface PM_{2.5}, the reanalysis meteorological data,
19 and the GEOS-Chem model simulation, we revealed the Transport-Nocturnal PM_{2.5} Enhancement by
20 Subsidence (T-NPES) events occurred frequently in the two cities, with percentages of 12.2 % and
21 18.0 %, respectively during Dec. 2018 - Feb. 2019. Furthermore, the GEOS-Chem model simulation
22 further confirmed ~~that~~ the ubiquity of winter T-NPES events ~~in~~ [on](#) a large scale including North China
23 Plain and [the](#) Yangtze River Delta. Process analysis revealed that the subsidence was closely correlated
24 with the southeasterly movement of the high-pressure system and the passage of the cold front, resulting
25 in the increase of temperature aloft, a stronger inversion layer, and further PM_{2.5} accumulation in the
26 atmospheric boundary layer. Thus, a conceptual model of the T-NPES events was proposed to highlight
27 this surface PM_{2.5} enhancement mechanism in these plain regions. However, it ~~was not applicable~~ [did not](#)
28 [apply](#) to the two cities in [the](#) basin region (Xi'an and Chengdu), due to the obstruction of the weather
29 system movement by the mountains surrounding the basin.

30 **1 Introduction**

31 The severe fine particulate matter (PM_{2.5}, particles with an aerodynamic diameter smaller than 2.5 μm)
32 pollution, caused by the rapid industrialization and urbanization in China (Guo et al., 2014; Huang et al.,
33 2014), has essential impacts on visibility, ecosystem, regional and global climates, and human health
34 (Yue et al., 2017; An et al., 2019; De Marco et al., 2019; Li et al., 2019b; Hao et al., 2021). To mitigate
35 the PM_{2.5} pollution, the government of China ~~has~~ implemented the Air Pollution Prevention and Control
36 Action Plan in 2013 by strict emission controls (Gao et al., 2020). ~~Despite~~ Despite the fact that the annual
37 average concentration of PM_{2.5} has ~~been~~ significantly decreased (Ding et al., 2019; Li et al., 2019a; Zhang
38 et al., 2019b; Silver et al., 2020; Geng et al., 2021b), the PM_{2.5} levels in the majority of Chinese cities
39 are still above the World Health Organization target (WHO, 2021). Particularly, the issue of PM_{2.5}
40 pollution remained critical in the North China Plain (NCP) and Yangtze River Delta (YRD) in winter
41 time (Peng et al., 2021; Qin et al., 2021).

42 The formation mechanisms of PM_{2.5} pollution were complex especially in China (Guo et al., 2014; Xiao
43 et al., 2021b). ~~such~~ Such as the high emission intensity (Zhang et al., 2019b), the rapid chemical
44 formation of secondary particles owing to the ~~gas-phase~~ gas phase and heterogeneous reactions (Wang et
45 al., 2017; Lu et al., 2019; Chen et al., 2020), and the interactions within the atmospheric boundary layer
46 (ABL) (Ding et al., 2013; Gao et al., 2016; Dong et al., 2017; Li et al., 2017). While the long-range
47 transport also had significant impacts on the PM_{2.5} pollution (Guo et al., 2014; Zhang et al., 2015; Huang
48 et al., 2018). Cold fronts, as a common synoptic circulation in winter, were usually ~~favourable~~ favorable
49 for the quick removal of the locally accumulated pollutants in the NCP (Zhao et al., 2013; Gao et al.,
50 2017), but conversely transport the pollutants to the YRD through a long distance (Kang et al., 2019;
51 Huang et al., 2020; Kang et al., 2021). Zhou et al. (2023) indicated that the cold fronts could transport
52 the precursors to the residual layer, where the secondary pollution was rapidly driven to be generated and
53 then exacerbate near-surface air pollution as a result of the development of the daytime convective ABL.
54 However, the above studies have focused on the impact of the horizontally transported pollutants on the
55 downstream regions after the passage of the cold front. ~~While~~ In comparison, few studies have been
56 conducted on the variation in the vertical direction of particulate matter in the ABL during the passage
57 of the cold front.

58 The vertical mixing exchange process between layer has great ~~impacts~~ impact on local air quality and
59 the subsidence motion is associated with the evolution of the inversion layer (Gramsch et al., 2014; Xu
60 et al., 2018; He et al., 2022). Zhang et al. (2022) reported that the PM_{2.5} concentration behind the cold

61 front increased due to the subsidence motion and inversion layer. Zhao et al. (2023) suggested that the
62 frontal downdrafts were an additional transport pathway in the nighttime to make [a](#) higher contribution
63 to the ground nitrate. Both of their studies were based on the model simulations, the observational
64 evidence of the subsidence behind the cold front and its impact on the nocturnal PM_{2.5} enhancement
65 events is still lacking. Shi et al. (2022) reported one subsidence case of particulate matter during the
66 passage of the cold front over Wangdu, China in winter, which revealed that the subsidence ~~was closely~~
67 ~~connect~~[was closely connected](#) to the enhancement of nocturnal PM_{2.5}.

68 To investigate the mechanisms of nocturnal PM_{2.5} enhancement triggered by subsidence, the three-
69 dimensional spatial and temporal distribution is crucial. Many field observations of the vertical
70 distribution of particulate matter have been performed employing various methods such as tethered
71 balloons (Wang et al., 2021; Ran et al., 2022), ~~airplane~~[airplanes](#) (Wang et al., 2018; Fast et al., 2022),
72 unmanned aerial vehicles (Song et al., 2021; Dubey et al., 2022) and the meteorological towers (Li et al.,
73 2022; Yin et al., 2023). Lidar, as an active remote sensing device with high temporal and spatial
74 resolution, has been extensively employed in atmospheric detection to obtain the profile of particulate
75 matter, wind, and temperature. The ground-based and satellite-based lidar have been widely used to
76 detect the vertical distribution of aerosol. In recent years, the mobile multi-lidar system has been
77 gradually developed and has become a powerful tool ~~to observe~~[for observing](#) ~~the development of~~
78 ~~species detection~~ in a vertical perspective. Compared with the traditional ground-lidar system, the mobile
79 multi-lidar system enables continuous mobile observations and provides information on the distribution
80 of specific factors along its path and can be used as an effective supplement to other fixed lidars.
81 Additionally, the mobile multi-lidar system can reach different cities by its portable setting in a short
82 time to carry out ~~the~~fixed-point observations. The mobile lidar system ~~had~~[has](#) been used to carry out
83 several observations in the past few years (Lv et al., 2020; He et al., 2021; Xu et al., 2022). He et al.
84 (2021) investigated the vertical distribution characteristics of particulate matter in the Guanzhong Plain
85 by using the mobile multi-lidar system. Xu et al. (2022) conducted an observational study on the three-
86 dimensional structure of particulate matter distribution in the Guangdong-Hong Kong-Macao Greater
87 Bay Area by using the mobile multi-lidar system and proposed a conceptual model to elucidate the
88 vertical distribution of particulate matter under different wind and temperature conditions.

89 Here, we conducted the first nationwide field measurements in winter 2018 using the mobile multi-lidar
90 system during winter 2018 in China, to investigate the vertical distribution characteristics of particulate
91 matter in different cities. We focus on the observed nocturnal PM_{2.5} enhancement events and seek insights

92 into their characteristics and ~~the~~ causes, by combining [with](#) the GEOS-Chem model simulation, the
93 surface PM_{2.5} observation_s and meteorological reanalysis dataset. Finally, we examine the ubiquity of
94 this phenomenon in plain regions in China and propose a conceptual model, providing detailed vertical
95 insights into the enhancement of nocturnal surface PM_{2.5}.

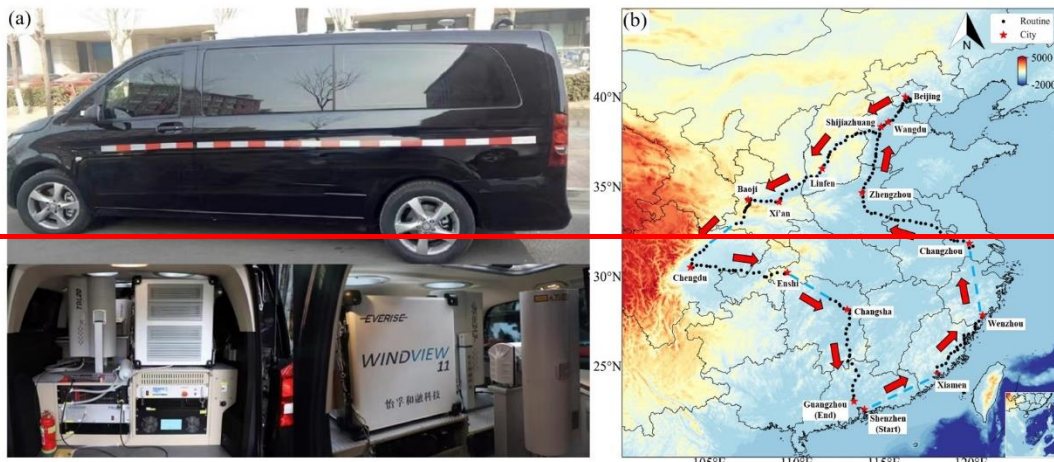
96 **2 Data and methods**

97 **2.1 Multi-lidar system**

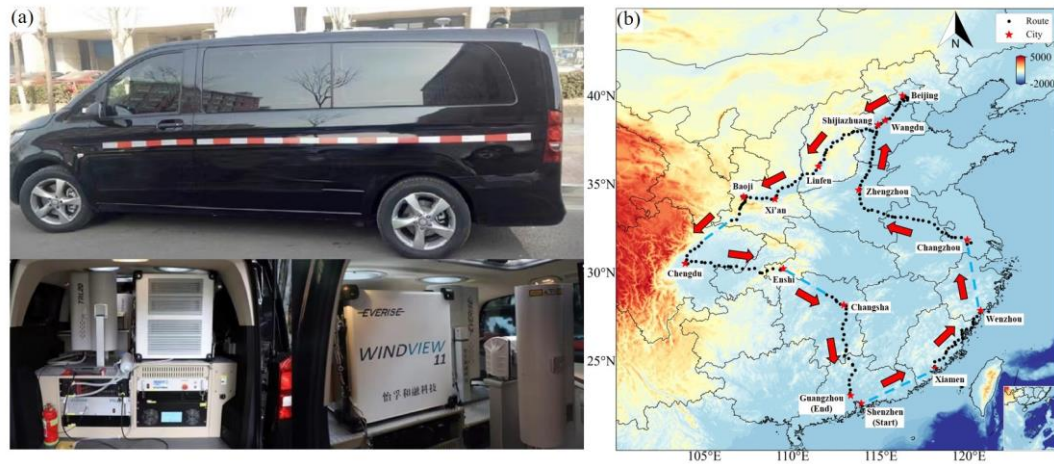
98 A multi-lidar system was installed on the mobile observation vehicle. The vehicle, a modified 7-seater
99 Mercedes-Benz sport utility vehicle, was equipped with three lidar instruments mounted on steel bars at
100 the rear for stability. The mobile observation routes were primarily on flat highways, and the speed was
101 controlled to remain around 80 km/h to minimize the impact of frequent changes in speed and vehicle
102 bumps on the measurement results.

103 The multi-lidar system (Everise Technology Ltd., Beijing) consisted of a 3D visual scanning micro pulse
104 lidar (EV-Lidar-CAM), a twirling Raman temperature profile lidar (TRL20), a Doppler wind profile lidar
105 (WINDVIEW10), a global positioning system (GPS). The 3D visual scanning ~~micro-pulse~~[micropulse](#)
106 lidar had a detection range of up to 30 km, a temporal resolution of 1 minute, and a vertical resolution of
107 15 m. ~~The 3D lidar emitted a 532 nm laser beam vertically, which is scattered by aerosol particles in the~~
108 ~~atmosphere~~ [The 3D lidar used an Nd: YAG laser to emit a 532 nm laser beam at a repetition frequency](#)
109 [of 2500 Hz, which is scattered by aerosol particles in the atmosphere](#). The backscattered signal is utilized
110 to calculate the aerosol extinction coefficient and depolarization ratio profile. The extinction coefficient
111 increases with higher particle pollution concentrations, while the depolarization ratio can distinguish
112 between spherical and non-spherical particles based on their size and shape. The Doppler wind profile
113 lidar provides a temporal resolution of 1 minute and a vertical resolution of 50 m. It emits a rotating 1545
114 nm laser beam [using a 10 kHz repetition rate](#) ~~fibre-pulse~~[fiber-pulse laser](#) and measures the Doppler shift
115 produced by the laser's backscattered signal as it passes through airborne particles such as dust, water
116 droplets in clouds and fog, polluted aerosols, salt crystals, and biomass-burning aerosols to derive the
117 horizontal and vertical wind speeds at any height. The Raman temperature profile lidar, based on Raman
118 scattering theory, calculates atmospheric temperature by detecting the rotational Raman scattering signal
119 of nitrogen or oxygen molecules in the atmosphere. Operating at a 532 nm wavelength [with an Nd: YAG](#)
120 [laser at a repetition frequency of 20 Hz](#), it has a temporal resolution of 5 minutes and a vertical resolution

121 of 60 m. The quality of the data obtained by the lidar system was checked by the Integrated
122 Environmental Meteorological Observation Vehicle before deployment. The results showed a percentage
123 difference of less than 15% between the lidar system data and the data provided by the Shenzhen
124 Meteorological Tower, demonstrating the high accuracy of the lidar instrument (Xu et al., 2022). [Data](#)
125 [during the instrument malfunction, below the blind zone, and in rainy weather had been excluded.](#)
126 Previous studies ~~had~~ [have](#) utilized this lidar system and demonstrated its reliability (Xu et al., 2018; He
127 et al., 2021). The mobile observation vehicle and multi-lidar system are shown in Figure 1(a). [The more](#)
128 [details of the multi-lidar system are shown in the Table S1.](#)



129



130

131 **Figure 1.** (a) The mobile observation vehicle and multi-lidar system. (b) ~~The~~ For the mobile observation route and
132 stopover cities, the blue dotted line shows the sections of missing data.

133 2.2 The route of nationwide mobile observation

134 To investigate the distribution characteristics of particulate matter during winter in different regions in
135 China, the Integrated Environmental Meteorological Observation Vehicle of Sun Yat-sen University was
136 utilized to conduct the first nationwide mobile observation campaign. The campaign, which lasted 43
137 days and covered approximately 11,000 km, started in Shenzhen on 30 November, 2018 and ended in
138 Guangzhou on 11 January, 2019. This campaign surveyed the $PM_{2.5}$ vertical profiles across 15 cities,
139 including Shenzhen, Xiamen, Wenzhou, Changzhou, Zhengzhou, Wangdu, Beijing, Shijiazhuang,
140 Linfen, Xi'an, Baoji, Chengdu, Enshi, Changsha and Guangzhou. The observation route and stopover
141 cities are shown in Figure 1(b). Due to the precipitation, there were no observations between Shenzhen-
142 Xiamen and Wenzhou-Changzhou, while some GPS data were missing between Beijing-Chengdu and
143 Enshi-Changsha.

144 To compare the vertical distribution characteristics of particulate matter in different regions, we
145 conducted fixed-point observations for several pollution days in four representative cities in the East
146 China region (Changzhou), North China Plain (Wangdu), Guanzhong Basin (Xi'an), and Sichuan Basin
147 (Chengdu). The dates and duration of the fixed-point observations are presented in Table 1. In the
148 following analysis, only the data obtained in the four fixed-point measurements are used since it has ~~an~~
149 enough time duration to show the vertical variation of $PM_{2.5}$.

150 **Table 1.** Date and cities of fixed-point observations

Date	Cities	Coordinate	Landform
2018.12.11-2018.12.14	Changzhou	119.97°E, 31.83°N	Plain area
2018.12.18-2018.12.22	Wangdu	115.25°E, 38.67°N	Plain area
2018.12.31-2019.01.02	Xi'an	109.01°E, 34.22°N	Basin area
2019.01.04-2019.01.09	Chengdu	103.92°E, 30.58°N	Basin area

151

152 2.3 Surface $PM_{2.5}$ data and ERA5 reanalysis data

153 The nationwide hourly observations of surface $PM_{2.5}$ in China are obtained from the China National
154 Environmental Monitoring Center (CNEMC) network (<https://quotsoft.net/air>, last accessed: March 2nd,

155 2023). Here, we used the hourly PM_{2.5} concentration data from the whole winter of 2018 (Dec. 2018 –
156 Feb. 2019) and selected data from the closest monitoring station to show the change in surface PM_{2.5}
157 concentration at the four observation sites.

158 The spatial distribution of daily average surface PM_{2.5} concentration is obtained from the TAP team
159 (<http://tapdata.org.cn>), with a spatial resolution of 10 km. Based on machine learning algorithms and
160 multi-source data information, the TAP team has built a multi-source data fusion system that integrates
161 ground observation data, satellite remote sensing information, high-resolution emission inventories, air
162 quality model simulations, and other multi-source information (Geng et al., 2021a; Xiao et al., 2021a).
163 In addition to the observation data, we also apply the three-dimensional meteorological data from [the](#)
164 ERA5 dataset for the winter of 2018 (<https://softnet.net/air>, last accessed: March 2nd, 2023) (Munoz-
165 Sabater et al., 2021). This dataset contained temperature, horizontal and vertical wind speed, and
166 direction at pressure levels, as well as two-dimensional data including sea-level pressure and 2-m
167 temperature. The ERA5 dataset is the fifth generation of the European Centre for Medium-Range
168 Weather Forecasts (ECMWF) atmospheric reanalysis of the global climate. The ERA5 dataset has a
169 horizontal resolution of 0.25°×0.25°, a vertical resolution of 25 hPa, and a temporal resolution of 1 h.

170 **2.4 HYSPLIT backward trajectory model**

171 The Hybrid Single Particle Lagrangian Integrated Trajectory Model (HYSPLIT) (Stein et al., 2015),
172 developed by NOAA Air Resources Laboratory, ~~which~~ is a valuable tool for simulating the movement
173 of air mass and the transport of pollutants in the atmosphere, is used in our study to obtain the sources of
174 particulate matter at different heights. Altitudes of 100, 500, and 1000 m were set as the ~~end~~
175 ~~points~~[endpoints](#) of the trajectories, the meteorological input for the trajectory model was the FNL dataset,
176 and each trajectory was calculated for 24 h duration.

177 **2.5 GEOS-Chem model description**

178 Given the short-term (less than one week) fixed-point observation duration of the mobile observation
179 vehicle in each city, we employ the global three-dimensional chemical transport model GEOS-Chem
180 version 13.3.1 to interpret the vertical observations (available at
181 <https://github.com/geoschem/GCClassic/tree/13.3.1>, last assessed: March 2nd, 2023, (Bey et al., 2001))
182 and to simulate the distribution of particulate matter concentrations during winter 2018 in China. We
183 perform the nested-grid version of [the](#) GEOS-Chem simulation at a spatial of 0.5° (latitude) × 0.625°

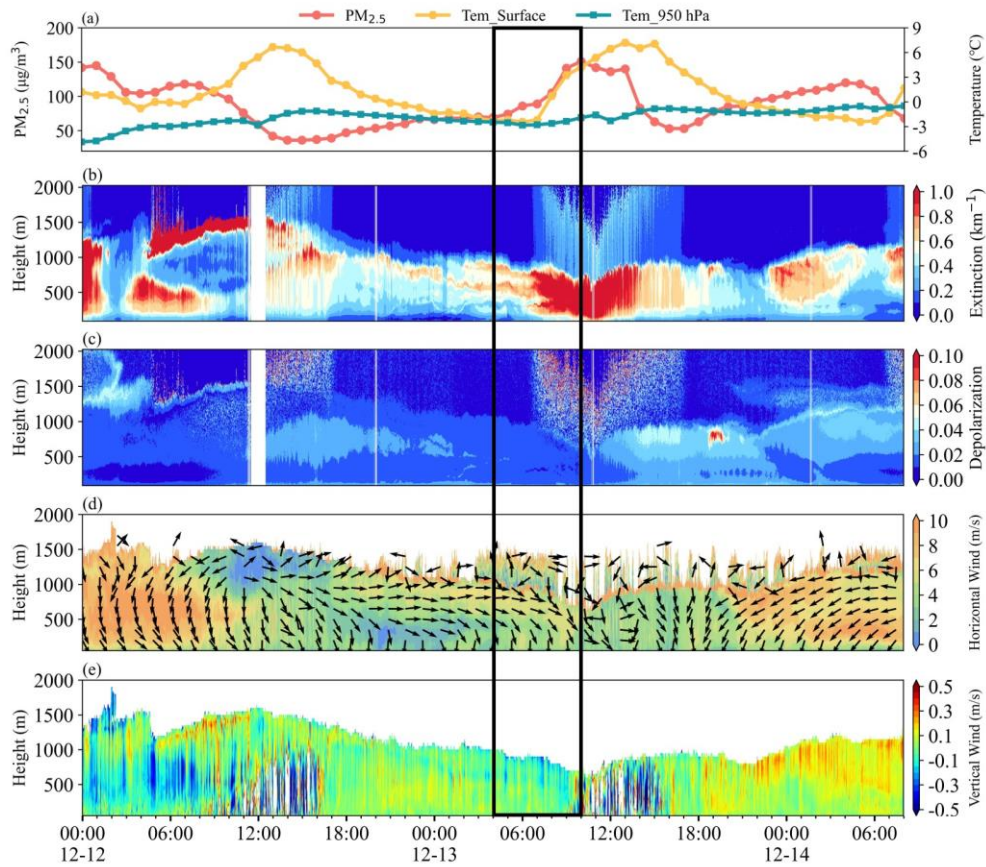
184 (longitude) resolution over East Asia (60-150°E, 11°S-55°N), The model has 47 vertical layers with 18
185 layers in the below 3 km. Boundary chemical conditions for the nested models are archived from a
186 consistent global simulation run at 4° latitude × 5° longitude resolution. Meteorological input is from the
187 Modern-Era Retrospective analysis for Research and Application version 2 (MERRA-2) (Gelaro et al.,
188 2017). We conduct the model simulation from 2018/11-2019/02 with the first ~~one~~-month as a spin-up.
189 The model mechanisms and emissions mostly follow our previous study (Wang et al., 2022). In short,
190 the GEOS-Chem model describes a comprehensive stratospheric and tropospheric ozone-NO_x-VOCs-
191 aerosol-halogen chemical mechanism (Wang et al., 1998; Park et al., 2004; Parrella et al., 2012; Mao et
192 al., 2013). Photolysis rates are computed using the Fast-JX scheme (Bian and Prather. 2002). Advection
193 of tracers in GEOS-Chem is accomplished through [the](#) TPCORE advection algorithm. ~~Boundary-The~~
194 [boundary](#) layer mixing process is described in (Lin and McElroy. 2010). Dry and wet deposition of both
195 gas and aerosols is considered (Wesely. 1989; Zhang et al., 2001). We apply the latest version of the
196 Community Emissions Data System (CEDSV2) anthropogenic emissions inventory (O'Rourke et al.,
197 2021) , in which the emissions over China have been adjusted to align with the Multi-resolution Emission
198 Inventory for China (MEIC) inventory (Zheng et al., 2018).
199 [Figure S1 showed the comparison of model results with observations for monthly mean PM_{2.5}, and the](#)
200 [correlation coefficients between model and observation were about 0.6, which meant that the model](#)
201 [results provided a relatively good reproduction of the observations.](#)

202 **3 Results and discussions**

203 **3.1 The observation of nocturnal PM_{2.5} enhancement in plain areas**

204 During the fixed-point observation in Changzhou, we observed a typical surface PM_{2.5} concentration
205 enhancement event starting at 4:00 and lasting until 10:00 on 13 December. As shown in Figure 2(a), the
206 concentration of PM_{2.5} increased from 69 to 151 µg/m³. Figure 2(b-c) ~~showed~~[shows](#) the spatiotemporal
207 distribution of the extinction coefficient and depolarization ratio. There was a clear layer with [a](#) low
208 extinction coefficient below 500 m from 16:00 on 12 December to 4:00 on 13 December, indicating low
209 PM_{2.5} concentration near the surface. Meanwhile, an aerosol layer with [a](#) high extinction coefficient of
210 about 0.7 km⁻¹ appeared at 500-1,000 m. Figure 2(d-e) depicted the west winds ~~prevailed~~[prevailing in](#)
211 the layer of 500-1,000 m with a wind speed (WS) of about 7 m/s. Based on the daily ~~averaged~~[average](#)
212 concentration of PM_{2.5} on 12 December shown in Figure [S2S1](#), the ~~west~~[western](#) area of the observation

213 site in Changzhou suffered from severe air pollution with the concentration of $PM_{2.5}$ exceeding $150 \mu\text{g}/\text{m}^3$.
214 Under the strong forcing of the west winds, the regional transport of aerosol from the west of Changzhou
215 was detected, leading to a high extinction coefficient layer at 500-1,000 m. The spatiotemporal
216 distribution of the vertical velocity in Figure 2(e) indicated the dominant updraft winds in the ABL,
217 which was conducive to the suspension of pollutants at 500-1,000 m.
218 However, the prevailing winds at 500-1,000 m shifted to the northwest/north after 4:00 on 13 December.
219 By 8:00, the north wind dominated in the ABL. The change in wind direction affected the transport
220 process of pollutants at 500-1,000 m, after which the transport basically disappeared. Meanwhile, the
221 downdraft winds dominated above 500 m (Figure 2(e)) and the aerosol layer suspended at ~~the~~ 500-1,000
222 m began to gradually transport and diffuse downward into the lower layer of ABL, which enhanced the
223 nocturnal surface $PM_{2.5}$ concentration. Noteworthy, after 4:00 on 13 December, the surface temperature
224 was close to the temperature at 950 hPa, suggesting that the structure of the ABL was stable and was
225 conducive to the accumulation of the $PM_{2.5}$.
226 The sea surface field showed the cold high-pressure system moved southeast with increasing strength
227 from 20:00, 12 December to 8:00, 13 December (Figure [S3S2](#)). The change in the synoptic weather
228 system was accompanied by a cold frontal passage. The cold frontal passage was inferred to start at about
229 4:00, 13 December and last about 4 hours, which was further illustrated by the clockwise rotation of the
230 horizontal wind from [the](#) ground to [the](#) upper layer (Shi et al., 2022) and the transition from updrafts to
231 downdrafts, the observation site was located behind the cold front after 4:00 where the descending
232 movements dominated. Under the influence of the subsidence, the pollutants transported by the west
233 advection diffused downward to the low layer and further aggravated the local air quality.

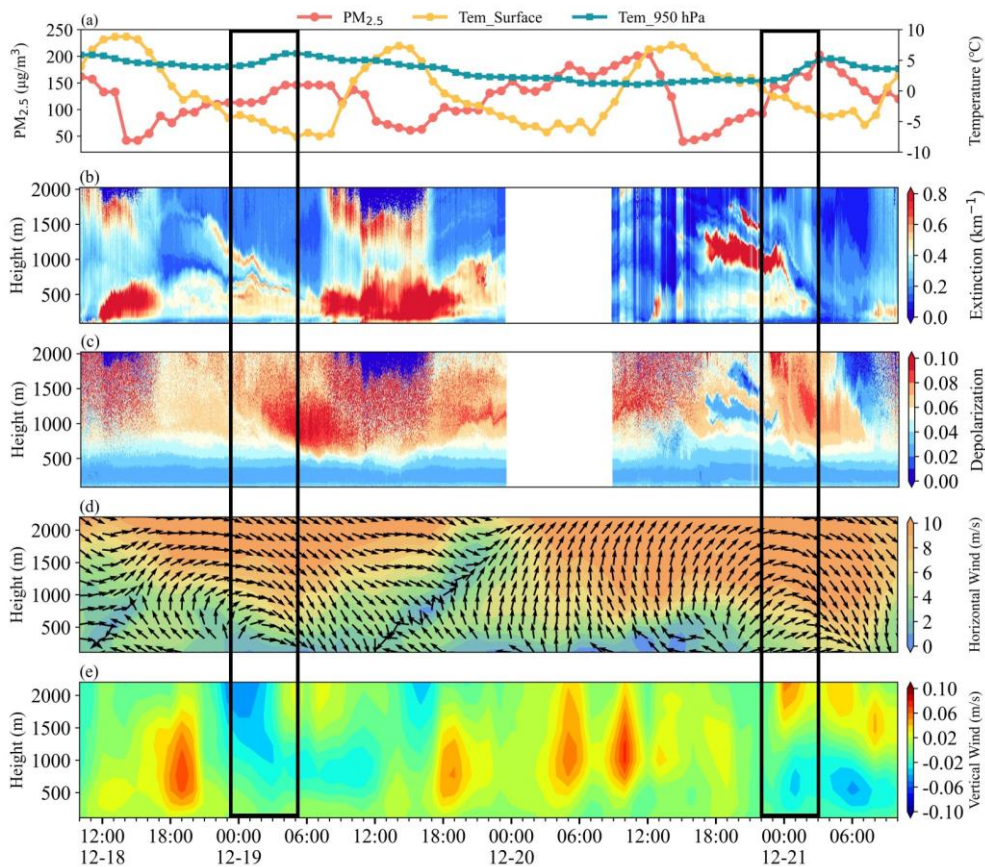


234

235 **Figure 2.** (a) Surface $PM_{2.5}$ concentration, surface temperature, and 950 hPa temperature, (b) Extinction coefficient,
 236 (c) Depolarization ratio, (d) Horizontal wind, and (e) Vertical wind, during the observation in Changzhou from 12
 237 December to 14 December. The black box indicated the nocturnal surface $PM_{2.5}$ enhanced event.

238 After 8:00, the concentration of surface $PM_{2.5}$ increased rapidly and peaked at around 10:00, the
 239 extinction coefficient below 1,000 m also reached a high level with 1.0 km^{-1} at the same time and the
 240 depolarization remained at about 0.01. The surface temperature began to rise and the convective ABL
 241 developed rapidly, which enhanced the vertical mixing and resulted in the rapid increase in surface $PM_{2.5}$
 242 (Zhou et al., 2023). And the north winds following the passage of the cold front dominated in the ABL
 243 after 8:00, which could bring pollution from the NCP to the YRD (Kang et al., 2019; Huang et al., 2020).
 244 Therefore, we attribute the increase in the concentration of surface $PM_{2.5}$ from 4:00 to 10:00 to the
 245 combination of the subsidence behind the cold front before 8:00, vertical mixing caused by the
 246 development of the convective ABL, and the transport by the north winds.

247 We also found similar nocturnal surface $PM_{2.5}$ enhancement events during the fixed-point observation in
248 Wangdu, on 19 December and 21 December respectively (Figure 3(a)). The concentration of $PM_{2.5}$
249 started to enhance at 1:00, 19 December, and meanwhile, the layer of pollutants above 1,000 m started
250 to transport and diffuse to the lower layer of ABL which was reflected by the change of the extinction
251 coefficient shown in Figure 3(b). Unfortunately, due to the instrument malfunction, the wind profile data
252 was unavailable and we used the ERA5 data instead, which previously showed good ~~consistent~~
253 consistency with the observation of with Doppler wind lidar (Shi et al., 2022). As shown in Figure 3(d),
254 from 10:00, 18 December to 0:00, 19 December, southwest winds prevailed above 1,000 m and the WS
255 exceeded 8 m/s, a persistent southerly wind could result in severe air pollution in the NCP (Cai et al.,
256 2017; Callahan et al., 2019; Zhang et al., 2019a). The wind forced the regional advection of pollutants
257 from the south region ~~suffered~~ suffering from serious air pollution (Figure ~~S4S3~~) to the observation site.
258 Meanwhile, the updrafts dominated in the ABL which facilitated the suspension of pollutants in the upper
259 layer. After 0:00, 19 December, as the cold high-pressure system moved southwest accompanied by a
260 cold front (Figure ~~S5S4~~), the prevailing winds above 1,000 m shifted to the northwest gradually and
261 downdrafts dominated behind the cold frontal passage. The changes in the horizontal and vertical wind
262 fields caused the advection of pollutants to disappear basically and the pollutants layer suspended above
263 1,000 m began to transport and diffuse downward to the low layer of ABL. The passage of the cold front
264 at 0:00, 19 December, lasted for 4 hours, and the subsidence behind the cold front caused the pollutants
265 to diffuse downward, enhancing the concentration of nocturnal $PM_{2.5}$.



266

267 **Figure 3.** (a) Surface PM_{2.5} concentration, surface temperature, and 950 hPa temperature, (b) Extinction coefficient,
 268 (c) Depolarization ratio, (d) Horizontal wind, and (e) Vertical wind, during the observation in Wangdu from 18
 269 December to 21 December. The black boxes indicated the Nocturnal PM_{2.5} enhancement events.

270 The pattern of the nocturnal surface PM_{2.5} enhancement event on 21 December was highly similar to that
 271 on 19 December. However, the pollutant advection process lasted a longer duration which started at
 272 16:00, 20 December and ended at 0:00, 21 December (Figure 3(b)), and the WS of the southwest wind
 273 above 1,000 m exceeded 12 m/s meeting the standard of the low-level jet (LLJ) (Kraus et al., 1985; Hu
 274 et al., 2013). The area south of the observation site in Wangdu suffered from more severe air pollution
 275 with the concentration of PM_{2.5} exceeding 300 $\mu\text{g}/\text{m}^3$ (Figure S6S5). Under the strong forcing of the
 276 ~~southwester~~ southwestern LLJ and the updrafts depicted in Figure 3(d-e), an aerosol layer with high
 277 extinction coefficient exceeding 2 km^{-1} formed and was suspended at 1,000-1,500 m from 16:00, 20
 278 December to 0:00, 21 December. Meanwhile, Figure 3(c) showed that the layer with low depolarization

279 was consistent with the layer with a high extinction coefficient, further ~~confirmed~~confirming the role of
280 transportation.

281 After 0:00, the wind direction of LLJ began to change due to the southeasterly movement of the high-
282 pressure system accompanied by a cold front (Figure ~~S7~~S6). The passage of the cold front started at 0:00,
283 21 December, and lasted for 4 hours, after which the downdrafts dominated below 1,500 m (Figure 3(e)),
284 and the ~~northwester~~northwestern LLJ no longer transported pollutants from the southern area but greatly
285 enhanced the turbulent mixing (Shi et al., 2022). Under the influence of the turbulence generated by LLJ
286 and subsidence behind the cold front, the aerosol-rich layer suspended at 1,000-1,500 m was gradually
287 transported and diffused downward into the lower layer of ABL, ultimately enhancing the concentration
288 of surface PM_{2.5}, which was consistent with the result reported by Shi et al. (2022), with the secondary
289 inorganic aerosol increasing simultaneously during the subsidence process as observed by the tethered
290 balloon.

291 Noteworthy, when both nocturnal surface PM_{2.5} enhancement events in Wangdu occurred, the
292 temperature at 950 hPa showed an increasing trend as a result of the heating of the air by compression as
293 it descended, while the surface temperature continuously declined (Figure 3(a)). The opposite variation
294 of surface temperature and temperature at 950 hPa stabilized the lower atmosphere. The stronger
295 inversion layer was probably induced by subsidence (Carlson and Stull, 1986). With the more ~~stably~~
296 stable atmospheric layer and inversion during subsidence, the concentration of surface PM_{2.5} enhanced
297 (Gramsch et al., 2014; Largeron and Staquet, 2016).

298 **3.2 Transport-Nocturnal PM_{2.5} Enhancement by Subsidence ~~events~~Events**

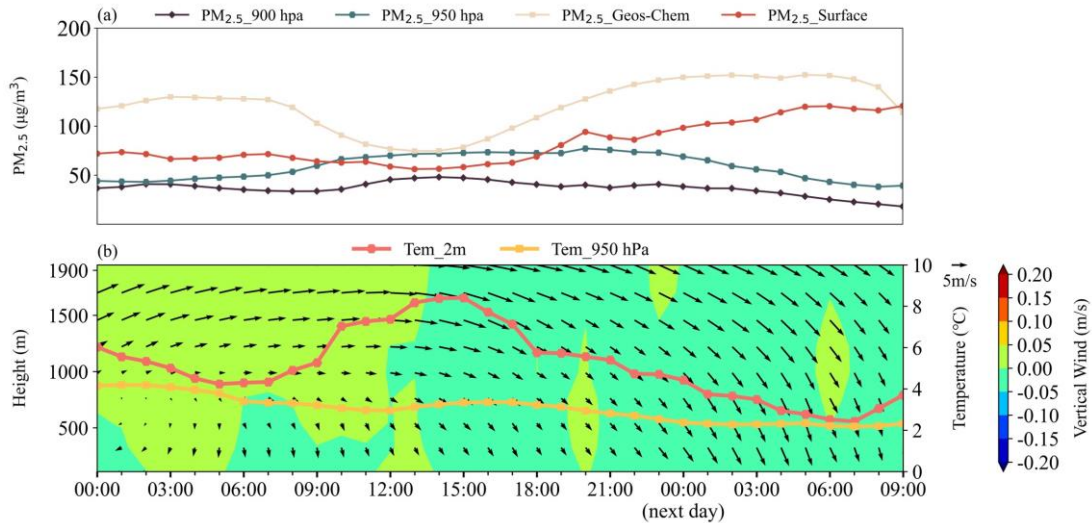
299 During the fixed-point observation, we found the causes of three nocturnal PM_{2.5} enhancement events in
300 different cities were similar. The processes ~~included~~can be summarized in the following as three steps:
301 First, the horizontal winds with high wind speed forced the transport of pollutants from the upstream
302 region, while the updrafts dominated, ~~both~~-resulting in the formation and suspension of an aerosol layer
303 with high extinction coefficient at the high layer of the ABL. Then, under the influence of the
304 southeasterly movement of the high-pressure system and the passage of the cold front, the horizontal
305 wind direction shifted to the north or northwest and the downdrafts became dominant. Finally, the
306 transport of pollutants disappeared due to the change of wind direction, and under the subsidence behind
307 the cold front, the aerosol-rich layer suspended at the high layer was gradually transported and diffused
308 downward into the lower layer of the ABL, ultimately enhancing the concentration of nocturnal PM_{2.5}.

309 Here, we defined this pollution pattern as T-NPES (Transport-Nocturnal PM_{2.5} Enhancement by
310 Subsidence) events.

311 To investigate the occurrence frequency of T-NPES events, we employed the GEOS-Chem model to
312 simulate the distribution of particulate matter concentrations in China during the whole winter of 2018
313 (Dec. 2018 – Feb. 2019). We utilized the simulated PM_{2.5} at 950 hPa and 900 hPa to represent the high-
314 altitude PM_{2.5} concentration. We selected the closest grid data of the wind field data, 950 hPa, and 2-m
315 temperature data from [the](#) ERA5 dataset to the observation site in Changzhou and Wangdu to show the
316 meteorological condition. By ~~analysing~~[analyzing](#) the hourly concentration variation of PM_{2.5} and the
317 distribution of the wind field during the three months of winter 2018 in Changzhou and Wangdu, we
318 found 11 typical T-NPES events in Changzhou accounting for 12.2% and 18 T-NPES events in Wangdu
319 accounting for 18%, which indicated that the T-NPES events were a relatively common phenomenon in
320 the two cities.

321 Figure 4 ~~showed~~[shows](#) the average pattern of all T-NPES events in Changzhou, the trend of the
322 simulated PM_{2.5} was consistent with the observation, confirming the credibility of the simulations. As
323 shown in Figure 4(a), the enhancement of nocturnal surface PM_{2.5} started at 21:00, when there was no
324 significant enhancement in anthropogenic PM_{2.5} emissions, while the high-altitude PM_{2.5} represented by
325 PM_{2.5} at 900 hPa and 950 hPa started to decrease, which was consistent with the observed event in
326 Changzhou described in Section 3.1. According to the distribution of [the](#) wind field (Figure 4(b)), west
327 winds with high wind speed prevailed [in](#) the layer above 1,000 m from 0:00 to about 18:00, which was
328 conducive to the transport of pollutants. ~~And the~~[The](#) updrafts dominated from 0:00 to 12:00, forcing the
329 pollutants suspending in the upper layer, which was reflected by the enhancing PM_{2.5} concentration at
330 ~~high-altitude~~[high altitude](#) (Figure 4(a)). Despite the downdrafts ~~dominated~~[dominating](#) after 12:00, there
331 was no immediate reduction in PM_{2.5} concentration at ~~high-altitude~~[high altitudes](#), which might be related
332 to the fact that the horizontal wind direction had not changed, and the transport of pollutants continued.
333 A brief updraft before 21:00 suspended the pollutants at ~~high-altitude~~[high altitudes](#). After 21:00,
334 northwester winds and downdrafts dominated in the ABL and the high-altitude PM_{2.5} began to gradually
335 transport and diffuse downward causing the enhancement of surface concentration of PM_{2.5}, and this
336 process continued until 4:00 in the next day. The surface temperature and the temperature at 950 hPa
337 gradually approached, which is consistent with the observed case in Changzhou, indicating that the
338 structure of the ABL was stable and was conducive to the accumulation of the PM_{2.5}. As shown in Figure
339 [S8S7](#), the average sea level pressure indicated that the southeasterly movement of the high-pressure

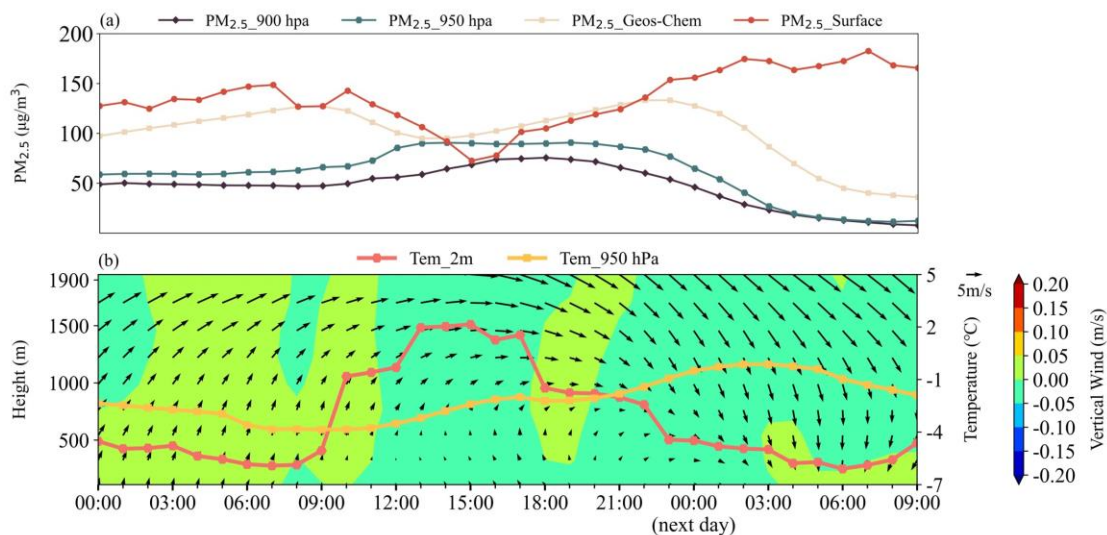
340 system and the passage of the cold front, which resulted in the shift in wind direction and subsidence
 341 behind the cold front, were the main causes of the T-NPES events.



342
 343 **Figure 4.** The average for all T-NPES events in Changzhou. (a) The concentration of PM_{2.5} at different levels,
 344 surface PM_{2.5} of observation (red line), surface PM_{2.5} of simulation (blue line), and PM_{2.5} at 900 hPa and 950 hPa.
 345 (b) The horizontal winds (arrows), the vertical winds (shaded), the temperature at 2 m, and temperature at 950 hPa.

346 Figure 5 ~~showed~~ shows the average pattern of all T-NPES events in Wangdu, which was similar to that
 347 in Changzhou. Figure 5(a) demonstrated that the trend of simulated PM_{2.5} was consistent with the
 348 observation before 22:00 but was different thereafter. The trend of high-altitude PM_{2.5} was increasing
 349 before 15:00 due to the transport of pollutants by prevailing southwester horizontal winds and the
 350 ~~dominant~~ dominance of updrafts which suspended the aerosol shown in ~~the~~ Figure 5(b). After 18:00, the
 351 prevailing winds began to turn ~~to~~ northwest and ultimately turn ~~to~~ north at 0:00 in the next day, while a
 352 brief updraft between 18:00 and 20:00 suspended the pollutants at ~~high altitude~~ high altitude. The ABL
 353 was dominated by the ~~northwester~~ northwestern winds and downdrafts after 21:00. Simultaneously, the
 354 high-altitude PM_{2.5} began to gradually transport and diffuse downward causing the enhancement of
 355 surface concentration of PM_{2.5}. The temperature at 950 hPa increased and the surface temperature
 356 declined (Figure 5(b)), which agreed with the two observation examples in Wangdu. The opposite
 357 variation of temperature at different ~~height~~ heights stabilized the ABL and further enhanced the
 358 concentration of PM_{2.5}. By ~~analysing~~ analyzing the weather circulation patterns, the causes of the T-

359 NPES events were the same ~~with~~as those in Changzhou and were attributed to the southeasterly
 360 movement of the high-pressure system and the passage of the cold front (Figure S9S8).
 361 Overall, the average patterns of T-NPES events in Changzhou and Wangdu were essentially in good
 362 agreement with the three cases of T-NPES in the two cities. But there were still slight differences, such
 363 as the change of Wangdu caused by the movement of high-pressure lasted a longer time in the average
 364 situation and the start time of subsidence behind the cold front was also not consistent, which were due
 365 to each T-NPES event was not exactly the same.



366
 367 **Figure 5.** The average for all T-NPES events in Wangdu. (a) The concentration of PM_{2.5} at different levels, surface
 368 PM_{2.5} of observation (red line), surface PM_{2.5} of simulation (blue line), and PM_{2.5} at 900 hPa and 950 hPa. (b) The
 369 horizontal winds (arrows), the vertical winds (shaded), the temperature at 2 m, and temperature at 950 hPa

370 3.3 The universality of T-NPES events in eastern China

371 Despite the mobile observation vehicle had no observations in other cities of the NCP, the YRD, and the
 372 Loess Plateau, we could still utilize the simulated data and the ERA5 data to investigate the universality
 373 of T-NPES events occurrence in other cities. We selected Shijiazhuang, Beijing, and Tianjin as
 374 represented cities of the NCP, Shanghai, and Nanjing as represented cities of the YRD, and Taiyuan,
 375 Linfen as represented cities of the Loess Plateau. We found ~~the~~a similar pattern of T-NPES events in all
 376 these cities. However, these T-NPES events in different cities had some differences in detail. Here we
 377 divided the T-NPES events into four types based on the status of PM_{2.5} after T-NPES events. More

378 information on the types, frequency of the T-NPES events, and their percentage of the winter 2018 was
 379 shown in Table 2.

380 The typical representation of Type 1 ~~was is~~ shown in Figure ~~S10S9~~, the characteristic of Type 1 was that
 381 the ~~southwester~~-southwestern winds transported the pollutants in ~~the~~ high-altitude of the ABL, then the
 382 wind direction shifted to north and downdrafts dominated, finally, pollutants in high-altitude diffused
 383 into lower layer causing the surface PM_{2.5} enhanced. However, after ~~the~~ T-NPES event, the north wind
 384 near the ground was not strong enough to remove the pollutants, causing ~~the a~~ high level of PM_{2.5} lasting
 385 the next day morning and may ~~resulting result~~ in aggravation of the air pollution in the following day.
 386 The characteristic of ~~the~~ T-NPES event of Type 2 was basically consistent with Type 1. However, after
 387 the T-NPES event, as north winds became stronger, pollutants were rapidly removed, resulting in a clean
 388 boundary layer throughout (Figure ~~S11S10~~). Even when the pollutants were removed more quickly by
 389 stronger north winds, the subsidence process might not be observed. Type 1 and Type 2 were both
 390 observed in the NCP cities, while Type 1 predominated in Wangdu and Shijiazhuang, and Type 2 in
 391 Beijing and Tianjin.

392 **Table 2.** Statistics of the T-NPES events in cities during Dec. 2018 – Feb. 2019

Area	Type	City	Frequency (days)	Percentages
NCP	Type 1 and 2	Wangdu	18	20.0%
		Shijiazhuang	18	20.0%
		Beijing	13	14.4%
		Tianjin	14	15.6%
YRD	Type 3	Changzhou	11	12.2%
		Shanghai	7	7.8%
		Nanjing	8	8.9%
Loess Plateau	Type 4	Linfen	18	20.0%
		Taiyuan	13	14.4%

393

394 Figure ~~S12S11 showed~~-shows the typical representation of Type 3. The prevailing wind transporting
 395 pollutants was not southwest but west and the start and end of the T-NPES event were later than for Type
 396 1 and 2. After the T-NPES event, the increase of 2-m temperature and the development of convective
 397 ABL led to ~~the~~-vertical mixing and the increase of surface PM_{2.5}. Additionally, the stronger north wind

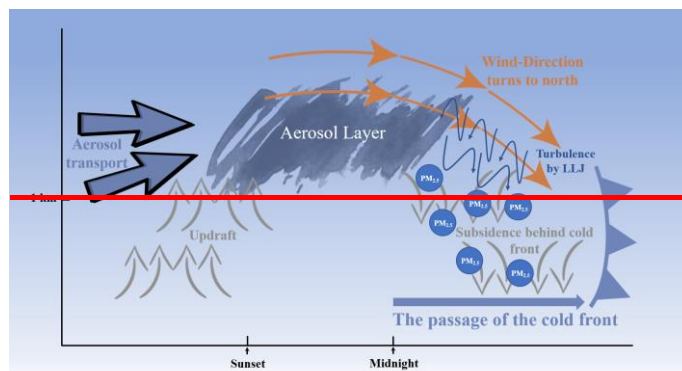
398 might transport the pollutants from the NCP to the YRD. ~~The~~Type 3 was similar to the example in
399 Changzhou in Section 3.1 and indicative of a typical pattern in the YRD cities.

400 The typical representation of Type 4, which ~~was~~ mainly occurred in the Loess Plateau cities, was shown
401 in Figure ~~S13~~~~S12~~. During the T-NPES event, the change of wind direction was only observed above
402 1,500 m while the wind speed below was so weak that the ~~shift~~~~shift~~ in wind direction was not significant,
403 which was significantly different from the wind field of the other three types. The reason for the
404 difference between Type 4 and other types was mainly related to the topography of the Loess Plateau,
405 which has a blocking effect on the movement of the high-pressure system. Noteworthy, after the analysis
406 of these T-NPES events in different cities in China, we suggested that the T-NPES events were a common
407 pattern of the nocturnal PM_{2.5} enhancement, but did not always have an impact on the air pollution of the
408 following day. The pollution levels on the following day depended more on the strength of the cold front,
409 local pollution conditions, the structure of ABL, and regional transportation. Further quantification is
410 needed to determine the relationship between the T-NPES events and the pollution levels on the
411 following day.

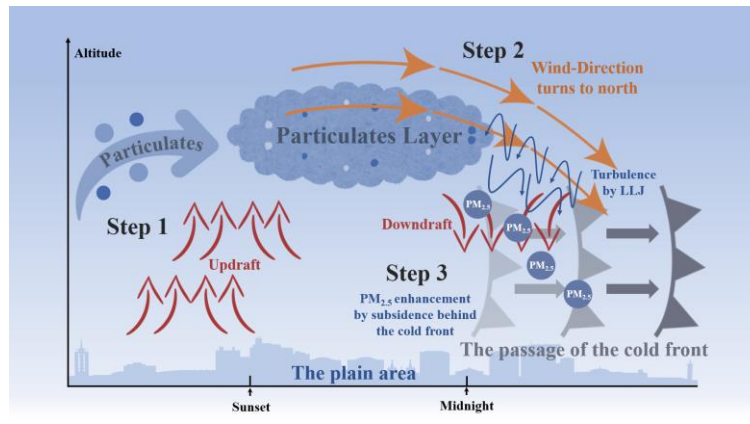
412 To ~~gain deeper~~ look insights into the mechanism of nocturnal PM_{2.5} enhancement, we systematically
413 documented instances of nocturnal PM_{2.5} enhancement during the winter of 2018 in Wangdu and
414 Changzhou according to the surface PM_{2.5} observation. We identified 48 such events in Wangdu and 27
415 in Changzhou, with proportions of T-NPES events of 37.5% and 40.7%, respectively. The results implied
416 that T-NPES represents merely one among multiple pathways contributing to the nocturnal PM_{2.5}
417 enhancement. We checked the nocturnal PM_{2.5} enhancement events that were not caused by T-NPES in
418 Wangdu, the dominant wind field distributions within the ABL were southerly or characterized by static
419 light wind, which indicated that the nocturnal PM_{2.5} enhancement might result from either horizontal
420 transport from polluted regions in the southern areas or the local accumulation of particulates in the stable
421 ABL. In the nocturnal PM_{2.5} enhancement events of non-T-NPES ~~condition~~conditions in Changzhou,
422 higher wind speeds in the ABL and predominantly from the northern and southwestern, which indicated
423 the nocturnal PM_{2.5} enhancement might result from horizontal transport from the NCP (Huang et al.,
424 2020) or caused by other reasons. For example, from the perspective of chemical formation, the nocturnal
425 atmospheric oxidation may elevate the nighttime aerosol concentration (Wang et al., 2023; Yan et al.,
426 2023). In addition, we found the T-NPES event does not always cause a nocturnal PM_{2.5} increase, in a
427 few cases, the strong north wind following the cold front play a role in ~~remove~~removing the aerosol. In
428 summary, the T-NPES just represents one vertical transport mechanism that can collectively

429 ~~contributes~~ contribute to the enhancement of nocturnal PM_{2.5} with other physical and chemical processes
430 (Zhao et al., 2023). Further understanding of the coupling effect of transportation as well as the chemical
431 formation to the nocturnal PM_{2.5} enhancement is thus highly needed.

432 Based on these mentioned above, we suggested that the T-NPES events were a common phenomenon in
433 winter in plain areas such as the NCP and the YRD. A conceptual model was thus developed and shown
434 in Figure 6, there ~~were~~ ~~was~~ the transportation of aerosol by the horizontal winds in the high altitude
435 ~~above 1,000 m~~ and the updrafts dominated before night, which was conducive to the formation and
436 suspension of the aerosol layer. Then, as with the southeasterly movement of the high-pressure system
437 and the passage of the cold front at about the time of midnight, the wind direction began to turn ~~to~~
438 north/northwest, causing the aerosol ~~diluted to dilute~~. Finally, the downdrafts dominated in the ABL and
439 the LLJ might enhance the ~~turbulent~~ turbulence. Under the influence of subsidence behind the cold front
440 and turbulence, the depth of the aerosol layer suspended in the high altitude ~~above 1,000 m~~ began to
441 decrease and the pollutants gradually transported and diffused downwards into the lower layer of the
442 ABL, enhancing the concentration of surface PM_{2.5}.



443



444

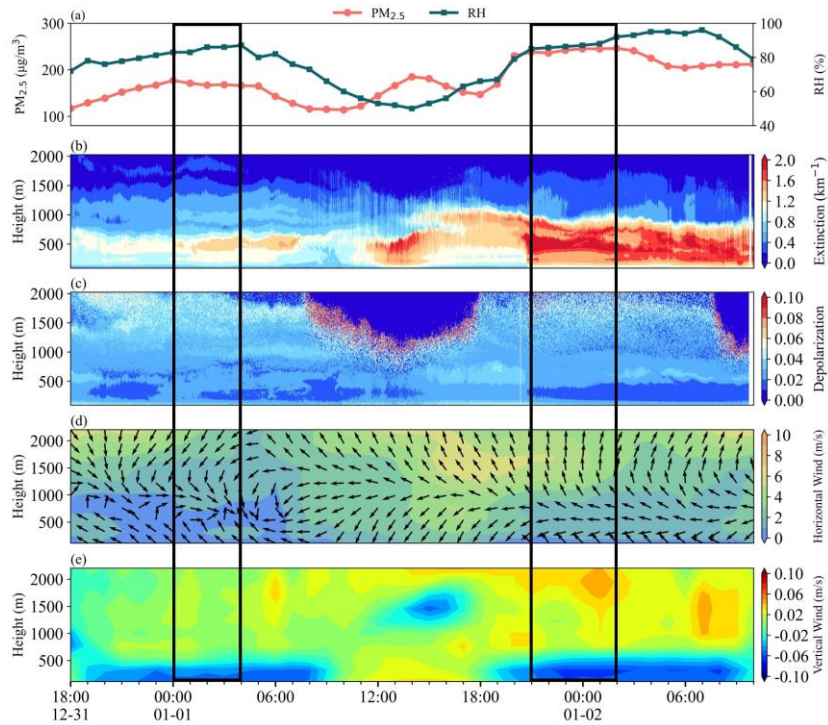
445 **Figure 6.** Conceptual scheme of the T-NPES events

446 **3.4 No T-NPES event occurred in Basin areas**

447 We further checked the fix-point measurement in Xi'an and Chengdu, two cities with typical basin
 448 topography. The results indicated that there were essentially no T-NPES events in either city, suggesting
 449 the ~~conceptual~~ concept did not work. Figure 7(a) indicated that the concentration of surface $PM_{2.5}$ had
 450 no enhancement during the night from 23:00 on 31 December to 4:00 on 1 January, and from 22:00 on
 451 1 January to 3:00 on 2 January in Xi'an. $PM_{2.5}$ remained at a high concentration, while the extinction
 452 coefficient did not show the subsidence process, suggesting that the T-NPES events were not common
 453 here.

454 Taking the night of 31 December as an example, from 18:00 on 31 December to 4:00 on 1 January, the
 455 concentration of surface $PM_{2.5}$ increased before 23:00 ~~and then stabilized~~. Then it stabilized at high
 456 values, while the extinction coefficient remained at a high level with about $1.0-1.2 \text{ km}^{-1}$ near 500 m. As
 457 shown in Figure 7(d), from 18:00, 31 December to 6:00, 1 January, a light wind layer appeared below
 458 1,000 m, with $\sim 1 \text{ m/s}$. Such a static and stable condition was conducive to the accumulation of locally
 459 generated particulate matter near the ground, causing the concentration of $PM_{2.5}$ to enhance between
 460 18:00 and 23:00 on 31 December and the formation and maintenance of the aerosol layer at about 500
 461 m. Noteworthy, the wind direction at the low layer was southeaster, while it was the opposite northwester
 462 at about 1,000 m, which was the typical characteristic of mountain-valley breeze circulation. The
 463 dominance of downdrafts below 500 m suggested that Xi'an was in the upper area of the nocturnal
 464 mountain-valley breeze circulation. The mountain-valley breeze circulation could only be observed when
 465 the background WS was relatively weak, which further indicated a stable structure of the ABL. The

466 example on 1 January was similar to the above one, with the extinction coefficient reaching 2 km^{-1} and
 467 [the](#) depolarization ratio decreasing after 21:00 due to the hygroscopic growth of aerosol by the rise in
 468 relative humidity.



469

470 **Figure 7.** (a) Surface $\text{PM}_{2.5}$ concentration and relative humidity, (b) Extinction coefficient, (c) Depolarization ratio,
 471 (d) Horizontal wind, and (e) Vertical wind, during the observation in Xi'an from 18:00, 31 December to 10:00, 2
 472 January. The two black boxes were the [time period](#) to be studied.

473 Due to the topography of the basin in Xi'an, the mountain-valley breeze circulation, or the horizontal
 474 winds with lower WS always dominated ~~in~~ the ABL, which was not conducive to the transport and
 475 dispersion of particulate matter. The stable structure of the ABL resulted in the particulate matter
 476 ~~accumulated~~ [accumulating](#) in the low layer, which was the main feature of the nocturnal particulate
 477 matter distribution in Xi'an.

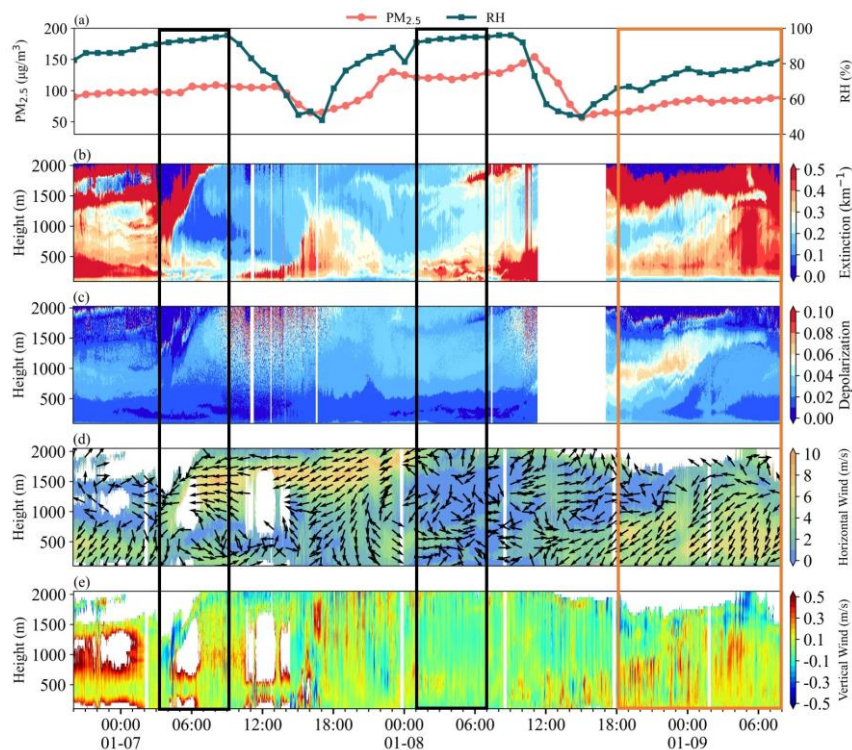
478 Figure 8 showed that the concentration of surface $\text{PM}_{2.5}$ also had no significant enhancement but
 479 remained a high value over nighttime in Chengdu. The distribution of the extinction coefficient in the
 480 two black boxes presented [a](#) double-layer structure, one layer near 250 m and another layer suspended at

481 about 500 m. Meanwhile, the wind field exhibited typical mountain-valley breeze circulation, as shown
482 in the two black boxes in Figure 8(d), which presented westerly wind near 250 m and southeasterly wind
483 above 500 m. The variation in wind direction due to the mountain-valley breeze circulation at different
484 ~~layer layers~~ might be responsible for the ~~double layer~~double layer of particulate matter. Figure ~~S14~~S13
485 ~~illustrated~~illustrates the backward trajectories when the double-layer appeared. The layer of particulate
486 matter at about 100 m might have originated from the southwest area of Chengdu, whereas the layer of
487 particulate matter at 500 m and 1,000 m might have originated from the northeast area of Chengdu. The
488 different sources of particulate matter were consistent with the mountain-valley breeze circulation in
489 Chengdu, further demonstrating the dominance of the mountain-valley breeze in the static and stable
490 ABL at night.

491 The orange box in Figure 8 indicated that the distribution of particulate matter in the ABL of Chengdu
492 under the dominance of northeasterly winds with high WS. Both the extinction coefficient and the
493 depolarization ratio showed a stratified structure, with the extinction coefficient initially higher below
494 750 m and lower above 750 m, whereas the depolarization ratio exhibited the opposite trend. The main
495 cause of this phenomenon was that the different sources of particulate matter in the two layers. Under
496 the influence of the dominant updrafts, local emissions with a high depolarization ratio were transported
497 upwards, while the lower layer was occupied by particulate matter with a lower depolarization ratio
498 transported by the northeasterly wind. As the continuous transport of the northeasterly wind, the entire
499 ABL was occupied by transported particulate matter with a high extinction coefficient and a low
500 depolarization ratio.

501 Due to the short time during the fixed-point observation period, it is difficult to make a universal
502 conclusion that no T-NEPS occurs in basin regions. Therefore, we further checked the surface and model
503 simulation data of the two basin cities for three months in winter 2018. We found that, unlike the plain
504 area, the T-NEPS events were ~~almost never~~rarely observed in the basin regions. It confirmed that the
505 conceptual model was indeed not applicable in the basin area. This was mainly attributed to the fact that
506 the movement of the weather system was blocked by the mountains surrounding the basin. Therefore,
507 the movement of the high-pressure system and the passage of the cold front had a weak impact on the
508 basin region. Without the downdrafts and the shift in wind direction associated with the movement of
509 the high-pressure system and the passage of the cold front, the structure of the ABL between Xi'an and
510 Chengdu was relatively stable, making it difficult for particulate matter to be transported and diffused,
511 and thus accumulate in the ABL at night. During the three months, we found that the wind field in Xi'an

512 was dominated by ~~the~~ light winds, while in Chengdu there were two states: one ~~is~~ was dominated by light
 513 winds and the other by strong northeasterly ~~wind~~ winds. Fortunately, our fixed-point observations had
 514 captured these typical processes indeed. In addition, considering the wind fields in basin cities were
 515 mainly dominated by light winds, which was the main characteristic ~~in~~ of basin area (Bei et al., 2016;
 516 Shu et al., 2021) and was similar to the wind fields below 1,500 m in Taiyuan and Linfen of the Type 4.
 517 Therefore, we suggested that the Loess Plateau cities might serve as a crucial transitional zone between
 518 the plains and the basin as introduced in Section 3.3. In summary, the conceptual model of T-NPES
 519 events was applicable to the plain areas which were more influenced by the movement of the weather
 520 system in winter, such as the NCP and YRD, but not to the basin areas.



521

522 **Figure 8.** (a) Surface PM_{2.5} concentration and relative humidity, (b) Extinction coefficient, (c) Depolarization ratio,
 523 (d) Horizontal wind, and (e) Vertical wind, during the observation in Chengdu from 20:00, 7 January to 8:00, 10
 524 January. The two black boxes were the ~~time period~~ period of the double-layer structure, the orange box was the ~~time~~
 525 ~~period~~ period to be studied.

526 **4 Conclusions and outlook**

527 In this study, we reveal that the T-NPES is a relatively common and important pathway that causes PM_{2.5}
528 pollution in the surface layer in ~~the~~ plain areas in winter China. The fixed-point observations in
529 Changzhou and Wangdu demonstrated that the T-NPES was associated with the subsidence of particulate
530 matter in the upper layer due to the movement of ~~high pressure~~ high pressure and the passage of the cold
531 front. Model simulations further confirmed the ubiquity of T-NPES events in plain areas, despite these
532 event types varied case by case. However, the observations in Xi'an and Chengdu indicated that the event
533 was less occurred in the basin areas, as the impact of the weather system was weakened by the obstruction
534 of mountains surrounding the basin. In ~~further~~ future studies, more multi-lidar ~~measurement~~
535 measurements should be conducted in other cities in the plains and basin areas to look insight to the
536 detailed mechanism of T-NPES events. In addition, more works are urgently needed to uncover the
537 vertical profiles of chemical components of the particulate matter, since it may also be affected by the
538 coupling of physical and chemical processes.

539 **Code/Data availability.** The datasets used in this study are available at:
540 <https://doi.org/10.5281/zenodo.8368944> (Wang et al., 2023).

541 **Author contributions.** H.C.W. and S.J.F designed the study. Y.M.W. and H.C.W. ~~analysed~~ analyzed
542 the data, H.L.W. and X.L. provided the GEOS-Chem model simulation results, and Y.M.W. and H.C.W.
543 wrote the paper with input from all coauthors.

544 **Competing interests.** The authors declare that they have no conflicts of interest.

545 **Acknowledgments.** The authors gratefully acknowledge the NOAA Air Resources Laboratory (ARL)
546 for the provision of the HYSPLIT transport and dispersion model used in this study.

547 **Financial support.** This research has been supported by the ~~Guangdong Major Project of Basic and~~
548 ~~Applied Basic Research (grant no. 2020B0301030004), the Guangdong science and technology plan~~
549 ~~project (grant no. 2019B121201002), and the National Natural Science Foundation of China (grant no.~~
550 ~~42175111)~~ Guangdong Major Project of Basic and Applied Basic Research (grant no.
551 2020B0301030004), the National Research Program for Key Issue in Air Pollution Control (grant No.
552 2023YFC3709201, 2023YFC3706103, 2023YFC3710900), and the National Natural Science

553 [Foundation of China \(grant no. 42175111\), the Fundamental Research Funds for the Central Universities,](#)
554 [Sun Yat-sen University \(23lgbj002\).](#)

555 **References**

- 556 An, Z.S., Huang, R.J., Zhang, R.Y., Tie, X.X., Li, G.H., Cao, J.J., Zhou, W.J., Shi, Z.G., Han, Y.M., Gu,
557 Z.L., Ji, Y.M.: Severe haze in northern China: A synergy of anthropogenic emissions and
558 atmospheric processes. *P. Natl. Acad. Sci. USA.* 116, 8657-8666.
559 <http://doi.org/10.1073/pnas.1900125116>, 2019
- 560 Bei, N.F., Xiao, B., Meng, N., Feng, T.: Critical role of meteorological conditions in a persistent haze
561 episode in the Guanzhong basin, China. *Sci. Total Environ.*, 550, 273-284.
562 <http://doi.org/10.1016/j.scitotenv.2015.12.159>, 2016
- 563 Bey, I., Jacob, D.J., Yantosca, R.M., Logan, J.A., Field, B.D., Fiore, A.M., Li, Q.B., Liu, H.G.Y.,
564 Mickley, L.J., Schultz, M.G.: Global modeling of tropospheric chemistry with assimilated
565 meteorology: Model description and evaluation. *J. Geophys. Res.: Atmos.*, 106, 23073-23095.
566 <http://doi.org/10.1029/2001JD000807>, 2001
- 567 Bian, H.S., Prather, M.J.: Fast-J2: Accurate simulation of stratospheric photolysis in global chemical
568 models. *J. Atmos. Chem.*, 41, 281-296. <http://doi.org/10.1023/A:1014980619462>, 2002
- 569 Cai, W.J., Li, K., Liao, H., Wang, H.J., Wu, L.X.: Weather conditions conducive to Beijing severe haze
570 more frequent under climate change. *Nat. Clim. Change.* 7, 257-+.
571 <http://doi.org/10.1038/NCLIMATE3249>, 2017
- 572 Callahan, C.W., Schnell, J.L., Horton, D.E.: Multi-Index Attribution of Extreme Winter Air Quality in
573 Beijing, China. *J. Geophys. Res.: Atmos.*, 124, 4567-4583.
574 <http://doi.org/10.1029/2018JD029738>, 2019
- 575 Carlson, M.A., Stull, R.B.: Subsidence in the nocturnal boundary layer. *J. Clim. Appl. Meteorol.*, 25,
576 1088-1099. [http://doi.org/10.1175/1520-0450\(1986\)025<1088:sitnbl>2.0.co;2](http://doi.org/10.1175/1520-0450(1986)025<1088:sitnbl>2.0.co;2), 1986
- 577 Chen, X.R., Wang, H.C., Lu, K.D., Li, C.M., Zhai, T.Y., Tan, Z.F., Ma, X.F., Yang, X.P., Liu, Y.H.,
578 Chen, S.Y., Dong, H.B., Li, X., Wu, Z.J., Hu, M., Zeng, L.M., Zhang, Y.H.: Field Determination
579 of Nitrate Formation Pathway in Winter Beijing. *Environ. Sci. Technol.*, 54, 9243-9253.
580 <http://doi.org/10.1021/acs.est.0c00972>, 2020

581 De Marco, A., Proietti, C., Anav, A., Ciancarella, L., D'Elia, I., Fares, S., Fornasier, M.F., Fusaro, L.,
582 Gualtieri, M., Manes, F., Marchetto, A., Mircea, M., Paoletti, E., Piersanti, A., Rogora, M.,
583 Salvati, L., Salvatori, E., Screpanti, A., Vialetto, G., Vitale, M., Leonardi, C.: Impacts of air
584 pollution on human and ecosystem health, and implications for the National Emission Ceilings
585 Directive: Insights from Italy. *Environ. Int.*, 125, 320-333.
586 <http://doi.org/10.1016/j.envint.2019.01.064>, 2019

587 Ding, A.J., Fu, C.B., Yang, X.Q., Sun, J.N., Petaja, T., Kerminen, V.M., Wang, T., Xie, Y., Herrmann,
588 E., Zheng, L.F., Nie, W., Liu, Q., Wei, X.L., Kulmala, M.: Intense atmospheric pollution
589 modifies weather: a case of mixed biomass burning with fossil fuel combustion pollution in
590 eastern China. *Atmos. Chem. Phys.*, 13, 10545-10554. [http://doi.org/10.5194/acp-13-10545-](http://doi.org/10.5194/acp-13-10545-2013)
591 [2013](http://doi.org/10.5194/acp-13-10545-2013), 2013

592 Ding, A.J., Huang, X., Nie, W., Chi, X.G., Xu, Z., Zheng, L.F., Xu, Z.N., Xie, Y.N., Qi, X.M., Shen,
593 Y.C., Sun, P., Wang, J.P., Wang, L., Sun, J.N., Yang, X.Q., Qin, W., Zhang, X.Z., Cheng, W.,
594 Liu, W.J., Pan, L.B., Fu, C.B.: Significant reduction of PM_{2.5} in eastern China due to regional-
595 scale emission control: evidence from SORPES in 2011-2018. *Atmos. Chem. Phys.*, 19, 11791-
596 11801. <http://doi.org/10.5194/acp-19-11791-2019>, 2019

597 Dong, Z.P., Li, Z.Q., Yu, X., Cribb, M., Li, X.M., Dai, J.: Opposite long-term trends in aerosols between
598 low and high altitudes: a testimony to the aerosol-PBL feedback. *Atmos. Chem. Phys.*, 17, 7997-
599 8009. <http://doi.org/10.5194/acp-17-7997-2017>, 2017

600 Dubey, R., Patra, A.K., Joshi, J., Blankenberg, D., Nazneen. Evaluation of vertical and horizontal
601 distribution of particulate matter near an urban roadway using an unmanned aerial vehicle. *Sci.*
602 *Total Environ.*, 836. <http://doi.org/10.1016/j.scitotenv.2022.155600>, 2022

603 Fast, J.D., Bell, D.M., Kulkarni, G., Liu, J.M., Mei, F., Saliba, G., Shilling, J.E., Suski, K., Tomlinson,
604 J., Wang, J., Zaveri, R., Zelenyuk, A.: Using aircraft measurements to characterize subgrid-
605 scale variability of aerosol properties near the Atmospheric Radiation Measurement Southern
606 Great Plains site. *Atmos. Chem. Phys.*, 22, 11217-11238. [http://doi.org/10.5194/acp-22-11217-](http://doi.org/10.5194/acp-22-11217-2022)
607 [2022](http://doi.org/10.5194/acp-22-11217-2022), 2022

608 Gao, M., Carmichael, G.R., Wang, Y., Saide, P.E., Yu, M., Xin, J., Liu, Z., Wang, Z.: Modeling study
609 of the 2010 regional haze event in the North China Plain. *Atmos. Chem. Phys.*, 16, 1673-1691.
610 <http://doi.org/10.5194/acp-16-1673-2016>, 2016

611 Gao, M., Liu, Z.R., Zheng, B., Ji, D.S., Sherman, P., Song, S.J., Xin, J.Y., Liu, C., Wang, Y.S., Zhang,
612 Q., Xing, J., Jiang, J.K., Wang, Z.F., Carmichael, G.R., McElroy, M.B.: China's emission
613 control strategies have suppressed unfavorable influences of climate on wintertime PM_{2.5}
614 concentrations in Beijing since 2002. *Atmos. Chem. Phys.*, 20, 1497-1505.
615 <http://doi.org/10.5194/acp-20-1497-2020>, 2020

616 Gao, M., Saide, P.E., Xin, J.Y., Wang, Y.S., Liu, Z.R., Wang, Y.X., Wang, Z.F., Pagowski, M.,
617 Guttikunda, S.K., Carmichael, G.R.: Estimates of Health Impacts and Radiative Forcing in
618 Winter Haze in Eastern China through Constraints of Surface PM_{2.5} Predictions. *Environ. Sci.*
619 *Technol.*, 51, 2178-2185. <http://doi.org/10.1021/acs.est.6b03745>, 2017

620 Gelaro, R., McCarty, W., Suarez, M.J., Todling, R., Molod, A., Takacs, L., Randles, C.A., Darmenov,
621 A., Bosilovich, M.G., Reichle, R., Wargan, K., Coy, L., Cullather, R., Draper, C., Akella, S.,
622 Buchard, V., Conaty, A., da Silva, A.M., Gu, W., Kim, G.K., Koster, R., Lucchesi, R., Merkova,
623 D., Nielsen, J.E., Partyka, G., Pawson, S., Putman, W., Rienecker, M., Schubert, S.D.,
624 Sienkiewicz, M., Zhao, B.: The Modern-Era Retrospective Analysis for Research and
625 Applications, Version 2 (MERRA-2). *J. Clim.*, 30, 5419-5454. [http://doi.org/10.1175/JCLI-D-](http://doi.org/10.1175/JCLI-D-16-0758.1)
626 [16-0758.1](http://doi.org/10.1175/JCLI-D-16-0758.1), 2017

627 Geng, G.N., Xiao, Q.Y., Liu, S.G., Liu, X.D., Cheng, J., Zheng, Y.X., Xue, T., Tong, D., Zheng, B.,
628 Peng, Y.R., Huang, X.M., He, K.B., Zhang, Q.: Tracking Air Pollution in China: Near Real-
629 Time PM_{2.5} Retrievals from Multisource Data Fusion. *Environ. Sci. Technol.*, 55, 12106-12115.
630 <http://doi.org/10.1021/acs.est.1c01863>, 2021a

631 Geng, G.N., Zheng, Y.X., Zhang, Q., Xue, T., Zhao, H.Y., Tong, D., Zheng, B., Li, M., Liu, F., Hong,
632 C.P., He, K.B., Davis, S.J.: Drivers of PM_{2.5} air pollution deaths in China 2002-2017. *Nat.*
633 *Geosci.*, 14, 645-+. <http://doi.org/10.1038/s41561-021-00792-3>, 2021b

634 Gramsch, E., Caceres, D., Oyola, P., Reyes, E., Vasquez, Y., Rubio, M.A., Sanchez, G.: Influence of
635 surface and subsidence thermal inversion on PM_{2.5} and black carbon concentration. *Atmos.*
636 *Environ.*, 98, 290-298. <http://doi.org/10.1016/j.atmosenv.2014.08.066>, 2014

637 Guo, S., Hu, M., Zamora, M.L., Peng, J.F., Shang, D.J., Zheng, J., Du, Z.F., Wu, Z., Shao, M., Zeng,
638 L.M., Molina, M.J., Zhang, R.Y.: Elucidating severe urban haze formation in China. *P. Natl.*
639 *Acad. Sci. USA.* 111, 17373-17378. <http://doi.org/10.1073/pnas.1419604111>, 2014

640 Hao, X., Li, J.D., Wang, H.J., Liao, H., Yin, Z.C., Hu, J.L., Wei, Y., Dang, R.J.: Long-term health impact
641 of PM_{2.5} under whole-year COVID-19 lockdown. *Environ. Pollut.*, 290.
642 <http://doi.org/10.1016/j.envpol.2021.118118>, 2021

643 He, C., Lu, X., Wang, H.L., Wang, H.C., Li, Y., He, G.W., He, Y.P., Wang, Y.R., Zhang, Y.L., Liu,
644 Y.M., Fan, Q., Fan, S.J.: The unexpected high frequency of nocturnal surface ozone
645 enhancement events over China: characteristics and mechanisms. *Atmos. Chem. Phys.*, 22,
646 15243-15261. <http://doi.org/10.5194/acp-22-15243-2022>, 2022

647 He, Y.P., Xu, X.Q., Gu, Z.L., Chen, X.H., Li, Y.M., Fan, S.J.: Vertical distribution characteristics of
648 aerosol particles over the Guanzhong Plain. *Atmos. Environ.*, 255.
649 <http://doi.org/10.1016/j.atmosenv.2021.118444>, 2021

650 Hu, X.-M., Klein, P.M., Xue, M., Zhang, F., Doughty, D.C., Forkel, R., Joseph, E., Fuentes, J.D.: Impact
651 of the vertical mixing induced by low-level jets on boundary layer ozone concentration. *Atmos.*
652 *Environ.*, 70, 123-130. <http://doi.org/10.1016/j.atmosenv.2012.12.046>, 2013

653 Huang, R.J., Zhang, Y.L., Bozzetti, C., Ho, K.F., Cao, J.J., Han, Y.M., Daellenbach, K.R., Slowik, J.G.,
654 Platt, S.M., Canonaco, F., Zotter, P., Wolf, R., Pieber, S.M., Bruns, E.A., Crippa, M., Ciarelli,
655 G., Piazzalunga, A., Schwikowski, M., Abbaszade, G., Schnelle-Kreis, J., Zimmermann, R., An,
656 Z.S., Szidat, S., Baltensperger, U., El Haddad, I., Prevot, A.S.H.: High secondary aerosol
657 contribution to particulate pollution during haze events in China. *Nature*. 514, 218-222.
658 <http://doi.org/10.1038/nature13774>, 2014

659 Huang, X., Ding, A.J., Wang, Z.L., Ding, K., Gao, J., Chai, F.H., Fu, C.B.: Amplified transboundary
660 transport of haze by aerosol-boundary layer interaction in China. *Nat. Geosci.*, 13, 428-+.
661 <http://doi.org/10.1038/s41561-020-0583-4>, 2020

662 Huang, X., Wang, Z.L., Ding, A.J.: Impact of Aerosol-PBL Interaction on Haze Pollution: Multiyear
663 Observational Evidences in North China. *Geophys. Res. Lett.*, 45, 8596-8603.
664 <http://doi.org/10.1029/2018GL079239>, 2018

665 Kang, H.Q., Zhu, B., Gao, J.H., He, Y., Wang, H.L., Su, J.F., Pan, C., Zhu, T., Yu, B.: Potential impacts
666 of cold frontal passage on air quality over the Yangtze River Delta, China. *Atmos. Chem. Phys.*,
667 19, 3673-3685. <http://doi.org/10.5194/acp-19-3673-2019>, 2019

668 Kang, H.Q., Zhu, B., Liu, X.H., Shi, S.S., Hou, X.W., Lu, W., Yan, S.Q., Pan, C., Chen, Y.: Three-
669 Dimensional Distribution of PM_{2.5} over the Yangtze River Delta as Cold Fronts Moving
670 Through. *J. Geophys. Res.: Atmos.*, 126. <http://doi.org/10.1029/2020JD034035>, 2021

671 Kraus, H., Malcher, J., Schaller, E.: A nocturnal low level jet during PUKK. Bound.-Layer Meteorol.
672 (Netherlands). 31, 187-195. <http://doi.org/10.1007/bf00121177>, 1985

673 Llargeron, Y., Staquet, C.: Persistent inversion dynamics and wintertime PM₁₀ air pollution in Alpine
674 valleys. Atmos. Environ., 135, 92-108. <http://doi.org/10.1016/j.atmosenv.2016.03.045>, 2016

675 Li, H.Y., Cheng, J., Zhang, Q., Zheng, B., Zhang, Y.X., Zheng, G.J., He, K.B.: Rapid transition in winter
676 aerosol composition in Beijing from 2014 to 2017: response to clean air actions. Atmos. Chem.
677 Phys., 19, 11485-11499. <http://doi.org/10.5194/acp-19-11485-2019>, 2019a

678 Li, L., Lu, C., Chan, P.W., Lan, Z.J., Zhang, W.H., Yang, H.L., Wang, H.C.: Impact of the COVID-19
679 on the vertical distributions of major pollutants from a tower in the Pearl River Delta. Atmos.
680 Environ., 276. <http://doi.org/10.1016/j.atmosenv.2022.119068>, 2022

681 Li, Z.Q., Guo, J.P., Ding, A.J., Liao, H., Liu, J.J., Sun, Y.L., Wang, T.J., Xue, H.W., Zhang, H.S., Zhu,
682 B.: Aerosol and boundary-layer interactions and impact on air quality. Natl. Sci. Rev., 4, 810-
683 833. <http://doi.org/10.1093/nsr/nwx117>, 2017

684 Li, Z.Q., Wang, Y., Guo, J.P., Zhao, C.F., Cribb, M., Dong, X.Q., Fan, J.W., Gong, D.Y., Huang, J.P.,
685 Jiang, M.J., Jiang, Y.Q., Lee, S.S., Li, H., Li, J.M., Liu, J.J., Qian, Y., Rosenfeld, D., Shan, S.Y.,
686 Sun, Y.L., Wang, H.J., Xin, J.Y., Yan, X., Yang, X., Yang, X.Q., Zhang, F., Zheng, Y.T.: East
687 Asian Study of Tropospheric Aerosols and their Impact on Regional Clouds, Precipitation, and
688 Climate (EAST-AIR(CPC)). J. Geophys. Res.: Atmos., 124, 13026-13054.
689 <http://doi.org/10.1029/2019JD030758>, 2019b

690 Lin, J.T., McElroy, M.B.: Impacts of boundary layer mixing on pollutant vertical profiles in the lower
691 troposphere: Implications to satellite remote sensing. Atmos. Environ., 44, 1726-1739.
692 <http://doi.org/10.1016/j.atmosenv.2010.02.009>, 2010

693 Lu, K.D., Fuchs, H., Hofzumahaus, A., Tan, Z.F., Wang, H.C., Zhang, L., Schmitt, S.H., Rohrer, F.,
694 Bohn, B., Broch, S., Dong, H.B., Gkatzelis, G.I., Hohaus, T., Holland, F., Li, X., Liu, Y., Liu,
695 Y.H., Ma, X.F., Novelli, A., Schlag, P., Shao, M., Wu, Y.S., Wu, Z.J., Zeng, L.M., Hu, M.,
696 Kiendler-Scharr, A., Wahner, A., Zhang, Y.H.: Fast Photochemistry in Wintertime Haze:
697 Consequences for Pollution Mitigation Strategies. Environ. Sci. Technol., 53, 10676-10684.
698 <http://doi.org/10.1021/acs.est.9b02422>, 2019

699 Lv, L., Xiang, Y., Zhang, T., Chai, W., Liu, W.: Comprehensive study of regional haze in the North
700 China Plain with synergistic measurement from multiple mobile vehicle-based lidars and a lidar
701 network. Sci. Total Environ., 721. <http://doi.org/10.1016/j.scitotenv.2020.137773>, 2020

702 Mao, J., Fan, S., Jacob, D.J., Travis, K.R.: Radical loss in the atmosphere from Cu-Fe redox coupling in
703 aerosols. *Atmos. Chem. Phys.*, 13, 509-519. <http://doi.org/10.5194/acp-13-509-2013>, 2013

704 Munoz-Sabater, J., Dutra, E., Agusti-Panareda, A., Albergel, C., Arduini, G., Balsamo, G., Boussetta, S.,
705 Choulga, M., Harrigan, S., Hersbach, H., Martens, B., Miralles, D.G., Piles, M., Rodriguez-
706 Fernandez, N.J., Zsoter, E., Buontempo, C., Thepaut, J.N.: ERA5-Land: a state-of-the-art global
707 reanalysis dataset for land applications. *Earth Syst. Sci. Data.* 13, 4349-4383.
708 <http://doi.org/10.5194/essd-13-4349-2021>, 2021

709 O'Rourke, P.R., Smith, S.J., Mott, A., Ahsan, H., McDuffie, E.E., Crippa, M., Klimont, S., McDonald,
710 B., Z., W., Nicholson, M.B., Feng, L., Hoesly, R.M., 2021. CEDS v-2021-04-21 Emission Data
711 1975-2019 (Version Apr-21-2021).

712 Park, R.J., Jacob, D.J., Field, B.D., Yantosca, R.M., Chin, M.: Natural and transboundary pollution
713 influences on sulfate-nitrate-ammonium aerosols in the United States: Implications for policy.
714 *J. Geophys. Res.: Atmos.*, 109. <http://doi.org/10.1029/2003JD004473>, 2004

715 Parrella, J.P., Jacob, D.J., Liang, Q., Zhang, Y., Mickley, L.J., Miller, B., Evans, M.J., Yang, X., Pyle,
716 J.A., Theys, N., Van Roozendaal, M.: Tropospheric bromine chemistry: implications for present
717 and pre-industrial ozone and mercury. *Atmos. Chem. Phys.*, 12, 6723-6740.
718 <http://doi.org/10.5194/acp-12-6723-2012>, 2012

719 Peng, J.F., Hu, M., Shang, D.J., Wu, Z.J., Du, Z.F., Tan, T.Y., Wang, Y.N., Zhang, F., Zhang, R.Y.:
720 Explosive Secondary Aerosol Formation during Severe Haze in the North China Plain. *Environ.*
721 *Sci. Technol.*, 55, 2189-2207. <http://doi.org/10.1021/acs.est.0c07204>, 2021

722 Qin, Y., Li, J.Y., Gong, K.J., Wu, Z.J., Chen, M.D., Qin, M.M., Huang, L., Hu, J.L.: Double high
723 pollution events in the Yangtze River Delta from 2015 to 2019: Characteristics, trends, and
724 meteorological situations. *Sci. Total Environ.*, 792.
725 <http://doi.org/10.1016/j.scitotenv.2021.148349>, 2021

726 Ran, L., Deng, Z.Z., Wu, Y.F., Li, J.W., Bai, Z.X., Lu, Y., Zhuoga, D.Q., Bian, J.C.: Measurement report:
727 Vertical profiling of particle size distributions over Lhasa, Tibet - tethered balloon-based in situ
728 measurements and source apportionment. *Atmos. Chem. Phys.*, 22, 6217-6229.
729 <http://doi.org/10.5194/acp-22-6217-2022>, 2022

730 Shi, Y., Zeng, Q.C., Liu, L., Huo, J.T., Zhang, Z., Ding, W.C., Hu, F.: Observed Evidence That
731 Subsidence Process Stabilizes the Boundary Layer and Increases the Ground Concentration of

732 Secondary Pollutants. *J. Geophys. Res.: Atmos.*, 127. <http://doi.org/10.1029/2021JD035244>,
733 2022

734 Shu, Z.Z., Liu, Y.B., Zhao, T.L., Xia, J.R., Wang, C.G., Cao, L., Wang, H.L., Zhang, L., Zheng, Y., Shen,
735 L.J., Luo, L., Li, Y.Q.: Elevated 3D structures of PM_{2.5} and impact of complex terrain-forcing
736 circulations on heavy haze pollution over Sichuan Basin, China. *Atmos. Chem. Phys.*, 21, 9253-
737 9268. <http://doi.org/10.5194/acp-21-9253-2021>, 2021

738 Silver, B., Conibear, L., Reddington, C.L., Knote, C., Arnold, S.R., Spracklen, D.V.: Pollutant emission
739 reductions deliver decreased PM_{2.5}-caused mortality across China during 2015-2017. *Atmos.*
740 *Chem. Phys.*, 20, 11683-11695. <http://doi.org/10.5194/acp-20-11683-2020>, 2020

741 Song, R.F., Wang, D.S., Li, X.B., Li, B., Peng, Z.R., He, H.D.: Characterizing vertical distribution
742 patterns of PM_{2.5} in low troposphere of Shanghai city, China: Implications from the perspective
743 of unmanned aerial vehicle observations. *Atmos. Environ.*, 265.
744 <http://doi.org/10.1016/j.atmosenv.2021.118724>, 2021

745 Stein, A.F., Draxler, R.R., Rolph, G.D., Stunder, B.J.B., Cohen, M.D., Ngan, F.: NOAA'S HYSPLIT
746 ATMOSPHERIC TRANSPORT AND DISPERSION MODELING SYSTEM. *Bull. Am.*
747 *Meteorol. Soc.*, 96, 2059-2077. <http://doi.org/10.1175/BAMS-D-14-00110.1>, 2015

748 Wang, D.F., Huo, J.T., Duan, Y.S., Zhang, K., Ding, A.J., Fu, Q.Y., Luo, J.H., Fei, D.N., Xiu, G.L.,
749 Huang, K.: Vertical distribution and transport of air pollutants during a regional haze event in
750 eastern China: A tethered mega-balloon observation study. *Atmos. Environ.*, 246.
751 <http://doi.org/10.1016/j.atmosenv.2020.118039>, 2021

752 Wang, F., Li, Z.Q., Ren, X.R., Jiang, Q., He, H., Dickerson, R.R., Dong, X.B., Lv, F.: Vertical
753 distributions of aerosol optical properties during the spring 2016 ARIAs airborne campaign in
754 the North China Plain. *Atmos. Chem. Phys.*, 18, 8995-9010. [http://doi.org/10.5194/acp-18-
755 8995-2018](http://doi.org/10.5194/acp-18-8995-2018), 2018

756 Wang, H.C., Lu, K.D., Chen, X.R., Zhu, Q.D., Chen, Q., Guo, S., Jiang, M.Q., Li, X., Shang, D.J., Tan,
757 Z.F., Wu, Y.S., Wu, Z.J., Zou, Q., Zheng, Y., Zeng, L.M., Zhu, T., Hu, M., Zhang, Y.H.: High
758 N₂O₅ Concentrations Observed in Urban Beijing: Implications of a Large Nitrate Formation
759 Pathway. *Environ. Sci. Technol. Lett.*, 4, 416-420. <http://doi.org/10.1021/acs.estlett.7b00341>,
760 2017

761 Wang, H.C., Wang, H.L., Lu, X., Lu, K.D., Zhang, L., Tham, Y.J., Shi, Z.B., Aikin, K., Fan, S.J., Brown,
762 S.S., Zhang, Y.H.: Increased night-time oxidation over China despite widespread decrease
763 across the globe. *Nat. Geosci.*, 16, 217-+. <http://doi.org/10.1038/s41561-022-01122-x>, 2023

764 Wang, Y.H., Logan, J.A., Jacob, D.J.: Global simulation of tropospheric O₃-NO_x-hydrocarbon
765 chemistry. 2. Model evaluation and global ozone budget. *J. Geophys. Res. (USA)*. 103, 10727-
766 10755. <http://doi.org/10.1029/98jd00157>, 1998

767 Wesely, M.L.: Parameterization of surface resistances to gaseous dry deposition in regional-scale
768 numerical models. *Atmos. Environ.*, 23, 1293-1304. [http://doi.org/10.1016/0004-
769 6981\(89\)90153-4](http://doi.org/10.1016/0004-6981(89)90153-4), 1989

770 WHO. WHO Global Air Quality Guidelines: Particulate Matter (PM_{2.5} and PM₁₀), Ozone, Nitrogen
771 Dioxide, Sulfur Dioxide and Carbon Monoxide, World Health Organization (WHO), Geneva,
772 Switzerland., 2021

773 Xiao, Q.Y., Geng, G.N., Cheng, J., Liang, F.C., Li, R., Meng, X., Xue, T., Huang, X.M., Kan, H.D.,
774 Zhang, Q., He, K.B.: Evaluation of gap-filling approaches in satellite-based daily PM_{2.5}
775 prediction models. *Atmos. Environ.*, 244. <http://doi.org/10.1016/j.atmosenv.2020.117921>,
776 2021a

777 Xiao, Q.Y., Zheng, Y.X., Geng, G.N., Chen, C.H., Huang, X.M., Che, H.Z., Zhang, X.Y., He, K.B.,
778 Zhang, Q.: Separating emission and meteorological contributions to long-term PM_{2.5} trends over
779 eastern China during 2000-2018. *Atmos. Chem. Phys.*, 21, 9475-9496.
780 <http://doi.org/10.5194/acp-21-9475-2021>, 2021b

781 Xu, X.Q., Xie, J.L., Li, Y.M., Miao, S.J., Fan, S.J.: Measurement report: Vehicle-based multi-lidar
782 observational study of the effect of meteorological elements on the three-dimensional
783 distribution of particles in the western Guangdong-Hong Kong-Macao Greater Bay Area.
784 *Atmos. Chem. Phys.*, 22, 139-153. <http://doi.org/10.5194/acp-22-139-2022>, 2022

785 Xu, Z.N., Huang, X., Nie, W., Shen, Y.C., Zheng, L.F., Xie, Y.N., Wang, T.Y., Ding, K., Liu, L.X.,
786 Zhou, D.R., Qi, X.M., Ding, A.J.: Impact of Biomass Burning and Vertical Mixing of Residual-
787 Layer Aged Plumes on Ozone in the Yangtze River Delta, China: A Tethered-Balloon
788 Measurement and Modeling Study of a Multiday Ozone Episode. *J. Geophys. Res.: Atmos.*,
789 123, 11786-11803. <http://doi.org/10.1029/2018JD028994>, 2018

790 Yan, C., Tham, Y.J., Nie, W., Xia, M., Wang, H.C., Guo, Y.S., Ma, W., Zhan, J.L., Hua, C.J., Li, Y.Y.,
791 Deng, C.J., Li, Y.R., Zheng, F.X., Chen, X., Li, Q.Y., Zhang, G., Mahajan, A.S., Cuevas, C.A.,

792 Huang, D.D., Wang, Z., Sun, Y.L., Saiz-Lopez, A., Bianchi, F., Kerminen, V.M., Worsnop,
793 D.R., Donahue, N.M., Jiang, J.K., Liu, Y.C., Ding, A.J., Kulmala, M.: Increasing contribution
794 of nighttime nitrogen chemistry to wintertime haze formation in Beijing observed during
795 COVID-19 lockdowns. *Nat. Geosci.*, 16, 975-+. <http://doi.org/10.1038/s41561-023-01285-1>,
796 2023

797 Yin, C.Q., Xu, J.M., Gao, W., Pan, L., Gu, Y.X., Fu, Q.Y., Yang, F.: Characteristics of fine particle
798 matter at the top of Shanghai Tower. *Atmos. Chem. Phys.*, 23, 1329-1343.
799 <http://doi.org/10.5194/acp-23-1329-2023>, 2023

800 Yue, X., Unger, N., Harper, K., Xia, X.G., Liao, H., Zhu, T., Xiao, J.F., Feng, Z.Z., Li, J.: Ozone and
801 haze pollution weakens net primary productivity in China. *Atmos. Chem. Phys.*, 17, 6073-6089.
802 <http://doi.org/10.5194/acp-17-6073-2017>, 2017

803 Zhang, G., Gao, Y., Cai, W.J., Leung, L.R., Wang, S.X., Zhao, B., Wang, M.H., Shan, H.Y., Yao, X.H.,
804 Gao, H.W.: Seesaw haze pollution in North China modulated by the sub-seasonal variability of
805 atmospheric circulation. *Atmos. Chem. Phys.*, 19, 565-576. [http://doi.org/10.5194/acp-19-565-](http://doi.org/10.5194/acp-19-565-2019)
806 [2019](http://doi.org/10.5194/acp-19-565-2019), 2019a

807 Zhang, L.M., Gong, S.L., Padro, J., Barrie, L.: A size-segregated particle dry deposition scheme for an
808 atmospheric aerosol module. *Atmos. Environ.*, 35, 549-560. [http://doi.org/10.1016/S1352-](http://doi.org/10.1016/S1352-2310(00)00326-5)
809 [2310\(00\)00326-5](http://doi.org/10.1016/S1352-2310(00)00326-5), 2001

810 Zhang, Q., Zheng, Y.X., Tong, D., Shao, M., Wang, S.X., Zhang, Y.H., Xu, X.D., Wang, J.N., He, H.,
811 Liu, W.Q., Ding, Y.H., Lei, Y., Li, J.H., Wang, Z.F., Zhang, X.Y., Wang, Y.S., Cheng, J., Liu,
812 Y., Shi, Q.R., Yan, L., Geng, G.N., Hong, C.P., Li, M., Liu, F., Zheng, B., Cao, J.J., Ding, A.J.,
813 Gao, J., Fu, Q.Y., Huo, J.T., Liu, B.X., Liu, Z.R., Yang, F.M., He, K.B., Hao, J.M.: Drivers of
814 improved PM_{2.5} air quality in China from 2013 to 2017. *P. Natl. Acad. Sci. USA.* 116, 24463-
815 24469. <http://doi.org/10.1073/pnas.1907956116>, 2019b

816 Zhang, R.Y., Wang, G.H., Guo, S., Zarnora, M.L., Ying, Q., Lin, Y., Wang, W.G., Hu, M., Wang, Y.:
817 Formation of Urban Fine Particulate Matter. *Chem. Rev.*, 115, 3803-3855.
818 <http://doi.org/10.1021/acs.chemrev.5b00067>, 2015

819 Zhang, W.H., Li, W.S., An, X.D., Zhao, Y.H., Sheng, L.F., Hai, S.F., Li, X.D., Wang, F., Zi, Z.F., Chu,
820 M.: Numerical study of the amplification effects of cold-front passage on air pollution over the
821 North China Plain. *Sci. Total Environ.*, 833. <http://doi.org/10.1016/j.scitotenv.2022.155231>,
822 2022

823 Zhao, X.J., Zhao, P.S., Xu, J., Meng, W., Pu, W.W., Dong, F., He, D., Shi, Q.F.: Analysis of a winter
824 regional haze event and its formation mechanism in the North China Plain. *Atmos. Chem. Phys.*,
825 13, 5685-5696. <http://doi.org/10.5194/acp-13-5685-2013>, 2013

826 Zhao, X.X., Zhao, X.J., Liu, P.F., Chen, D., Zhang, C.L., Xue, C.Y., Liu, J.F., Xu, J., Mu, Y.J.: Transport
827 Pathways of Nitrate Formed from Nocturnal N₂O₅ Hydrolysis Aloft to the Ground Level in
828 Winter North China Plain. *Environ. Sci. Technol.* <http://doi.org/10.1021/acs.est.3c00086>, 2023

829 Zheng, B., Tong, D., Li, M., Liu, F., Hong, C.P., Geng, G.N., Li, H.Y., Li, X., Peng, L.Q., Qi, J., Yan,
830 L., Zhang, Y.X., Zhao, H.Y., Zheng, Y.X., He, K.B., Zhang, Q.: Trends in China's
831 anthropogenic emissions since 2010 as the consequence of clean air actions. *Atmos. Chem.*
832 *Phys.*, 18, 14095-14111. <http://doi.org/10.5194/acp-18-14095-2018>, 2018

833 Zhou, X., Huang, X., Sun, P., Chi, X., Ren, C., Lai, S., Wang, Z., Qi, X., Wang, J., Nie, W., Xu, Z., Huo,
834 J., Fu, Q., Ding, A.: Fast Secondary Aerosol Formation in Residual Layer and Its Impact on Air
835 Pollution Over Eastern China. *J. Geophys. Res.: Atmos.*, 128, e2023JD038501.
836 <http://doi.org/https://doi.org/10.1029/2023JD038501>, 2023

837